Multiobjective-Optimization-Based Transmit Beamforming for Multitarget and Multiuser MIMO-ISAC Systems

Chunwei Meng, Zhiqing Wei, *Member, IEEE*, Dingyou Ma, Wanli Ni, *Member, IEEE*, Liyan Su, and Zhiyong Feng, *Senior Member, IEEE*

***Abstract*—Integrated sensing and communication integrated sensing and communications (ISAC) is an enabling technology for the sixth-generation mobile communications, which equips the wireless communication networks with sensing capabilities. In this article, we investigate transmit beamforming design for the multiple-input and multiple-output (MIMO)-ISAC systems in scenarios with multiple radar targets and communication users. A general form of multitarget sensing mutual information (MI) is derived, along with its upper bound, which can be interpreted as the sum of individual single-target sensing MI. Additionally, this upper bound can be achieved by suppressing the cross-correlation among the reflected signals from different targets, which aligns with the principles of adaptive MIMO radar. Then, we propose a multiobjective optimization framework based on the signal-to-interference-plus-noise ratio of each user and the tight upper bound of sensing MI, introducing the Pareto boundary to characterize the achievable communication-sensing performance boundary of the proposed ISAC system. To achieve the Pareto boundary, the max-min system utility function method is employed, while considering the fairness between the communication users and radar targets. Subsequently, the bisection search method is employed to find a specific Pareto optimal solution by solving a series of convex feasible problems. Finally, the simulation results validate that the proposed method achieves a better tradeoff between the multiuser communication and multitarget sensing performance. Additionally, utilizing the tight upper bound of sensing MI as a performance metric can enhance the multitarget resolution capability and angle estimation accuracy.**

***Index Terms*—Integrated sensing and communications (ISAC), multiple-input and multiple-output (MIMO), mutiobjective optimization, mutual information (MI), transmit beamforming.**

Manuscript received 14 May 2024; accepted 9 June 2024. Date of publication 13 June 2024; date of current version 6 September 2024. This work was supported in part by the National Natural Science Foundation of China (NSFC) under Grant 92267202 and Grant 62321001; in part by the National Key Research and Development Program of China under Grant 2020YFA0711303; in part by the Beijing Natural Science Foundation under Grant Z220004; and in part by the Fundamental Research Funds for the Central Universities under Grant 2024RC02. *(Corresponding author: Zhiqing Wei; Zhiyong Feng.)*

Chunwei Meng, Zhiqing Wei, Dingyou Ma, and Zhiyong Feng are with the Key Laboratory of Universal Wireless Communications, Ministry of Education, Beijing University of Posts and Telecommunications, Beijing 100876, China (e-mail: mengchunwei@bupt.edu.cn; weizhiqing@bupt.edu.cn; dingyouma@bupt.edu.cn; fengzy@bupt.edu.cn).

Wanli Ni is with the Department of Electronic Engineering, Tsinghua University, Beijing 100084, China (e-mail: niwanli@tsinghua.edu.cn).

Liyan Su is with the Research Department, Beijing RD Subdivision, Wireless Network, Huawei Technologies Company Ltd., Beijing 100085, China (e-mail: suliyan1@huawei.com).

Digital Object Identifier 10.1109/JIOT.2024.3413687

I. Introduction

THE NEXT-GENERATION wireless networks (6G and 5G-beyond) have been envisioned as a vital enabler for numerous emerging applications, such as autonomous vehicles, smart cities, and Internet of Things [1], [2]. The challenging problem is to satisfy the requirements of these applications for efficient communication and high-accuracy sensing, which motivates the development of frameworks for communication-sensing integration. As such, ISAC has been proposed as an appealing technology and has attracted great research interests recently [2], [3], [4], [5], [6]. In particular, ISAC can significantly enhance the spectral efficiency and reduce the hardware software complexity by sharing the hardware platform and the resources in spatial, temporal as well as the frequency domains for both communication and sensing [3], [7], [8].

The MIMO technique plays a significant role in the ISAC systems, which enables spatial multiplexing, diversity, and beamforming, leading to higher data rates, improved link reliability, enhanced spatial resolution, and accurate target parameter estimation [9], [10]. However, the inherent difference between communication and sensing leads to compromised performance, posing challenges for the MIMO-ISAC systems. Therefore, the key issue is to design effective transmit beamforming strategies that can flexibly balance the performance of both the functionalities while catering to the diverse requirements in practical scenarios. Numerous studies have investigated the joint optimization of transmit beamforming by considering both the communication and sensing performance metrics [11], [12], [13], [14], [15], [16], [17], [18], [19], [20], [21]. The work of [14] optimized the transmit beamforming by maximizing the peak sidelobe level of radar while ensuring given signal-to-interference-plus-noise ratio (SINR) threshold levels for the users. Furthermore, the studies conducted in [12] and [13] decomposed the transmit waveform into radar and communication waveform, and optimize the beamformers for each waveform to satisfy the respective performance requirements for sensing and communication. Additionally, in the context of specific sensing tasks, such as target estimation and tracking, some literature employs the Cramèr-Rao bound (CRB) as a performance metric to evaluate the estimation performance of the target parameters [18], [19], [20]. Liu et al. [18] minimized CRB

on the parameter estimates for a single target while ensuring the predefined communication SINR threshold for each downlink user. Then, Ren et al. [20] minimized the multitarget estimation CRB, subject to the minimum communication requirement. However, the lower bound for estimation accuracy provided by CRB may be not tight at low signal-to-noise ratio (SNR), and its complex and nonconvex mathematical nature always results in a more challenging optimization problem.

As a comparison, MI is also a commonly used sensing performance metric, which provides accurate estimation and classification capabilities in a more concise form [8] and [22]. Tang and Li [23] demonstrated that the optimal waveform designed by maximizing sensing MI enables efficient coexistence of the MIMO radar and communication systems occupying the same spectrum. Yang and Blum [24] showed that under the assumption of the Gaussian distributed target response, maximizing MI and maximizing minimum mean square error (MMSE) lead to the same optimal waveform solution. In [15], the emphasis on the accuracy of entire sensing channel vectors with sensing MI enhances overall sensing performance beyond the focus on the specific parameter-associated partial channels with the CRB. Chen et al. [25] showed that maximizing sensing MI through the waveform design improved the target detection and feature extraction performance. Besides, the similarity between the communication and sensing MI expressions also facilitates the efficient tradeoff between the two functionalities through the weighted sum optimization [16], [26]. Yuan et al. [16] optimized a weighted sum of communication and sensing MI to improve the balanced performance of both the functionalities. Dong et al. [27] established a relationship between the sensing MI and the rate-distortion theory, imparting operational estimation theoretic meaning to the MI-based methods. Furthermore, [28] demonstrated that the MI-based beamforming design can effectively suppress echo interference from scatters in the surrounding environment.

Simultaneously supporting multiuser communication and multitarget sensing in practical scenarios poses a critical challenge for the MIMO-ISAC systems [14], [20]. Such scenarios are inherently complex due to the diverse performance requirements for both communication and sensing. Moreover, they involve multiple intrinsic tradeoffs, such as the performance tradeoffs among the multiple communication users, multiple sensing targets, and between communication and sensing. Therefore, it is essential to develop a beamforming method that can flexibly balance multiuser communication and multitarget sensing performance based on their respective priorities. Given its advantages in enhancing target detection, estimation, and classification performance in a concise manner, sensing MI serves as a more suitable performance metric for multitarget sensing, as mentioned before [15], [16], [17], [25], [26], [27], [28]. However, existing research based on sensing MI still has some limitations. First, sensing MI in current studies offers a general overview of the sensing channel containing the multitarget information, but lacks a clear and detailed characterization of multitarget sensing performance and the relationships between the targets. Second, the lack of precise depiction of achievable performance boundaries for communication and sensing hinders the attainment of optimal performance tradeoffs. Furthermore, the absence of fairness consideration between the users and targets poses limitations on meeting diverse and specific requirements, thereby impeding the flexibility of beamforming designs.

To address these limitations, we propose a novel transmit beamforming approach for the multiuser multitarget MIMO-ISAC systems based on the sensing MI and communication SINRs. We consider a scenario where the base station (BS) communicates with multiple downlink users while sensing multiple targets simultaneously. To fully exploit the degrees of freedom (DoF)s provided by MIMO to meet the performance requirements of both multiuser communication and multitarget sensing, we synthesize communication and radar signals, and then jointly design their respective transmit beamforming [12], [13], [18]. Then, we derive a general expression for sensing MI and its tight upper bound to explore the structural features of maximum sensing MI. We find that maximizing the MI upper bound under zero-forced cross-correlation constraints aligns with the principles of the adaptive MIMO radar technique [29]. Therefore, we utilize the constrained upper bound of sensing MI as the performance metric for multitarget sensing, each user's SINR as the communication performance metric, and construct a multiobjective optimization problem (MOOP) to comprehensively investigate the tradeoff in communication-sensing performance. To efficiently solve the MOOP, we define the achievable performance region and its Pareto boundary. Then, we formulate a max-min utility optimization problem to obtain a specific Pareto solution for the MOOP, and utilize the properties of the achievable performance region to prove that the optimal solution of this max-min problem lies on the Pareto boundary. Finally, a bisection search method is employed to find the Pareto optimal solution for a specific set of communication-sensing weights. The main contributions of this article are summarized as follows.

1) We derive a novel general form of multitarget sensing MI and alongside a tight upper bound that satisfies zero-forced cross-correlation constraints. Furthermore, by suppressing the cross-correlation among the signals reflected from different targets, not only can sensing MI reach its maximum but the signals can also be considered independent of each other, which benefits target detection and tracking. Remarkably, we find that the upper bound of sensing MI can be viewed as the sum of single-target sensing MI, resembling a concise form similar to communication sum-rate and simplifying subsequent optimization processes.
2) To comprehensively investigate the tradeoff in communication and sensing performance, we formulate a MOOP to simultaneously optimize communication SINRs and sensing MI. Then, we introduce the Pareto boundary of the MOOP to characterize the achievable performance boundary of the proposed ISAC system. To obtain a specific set of Pareto solutions, a max-min utility function method is employed, which can be solved through

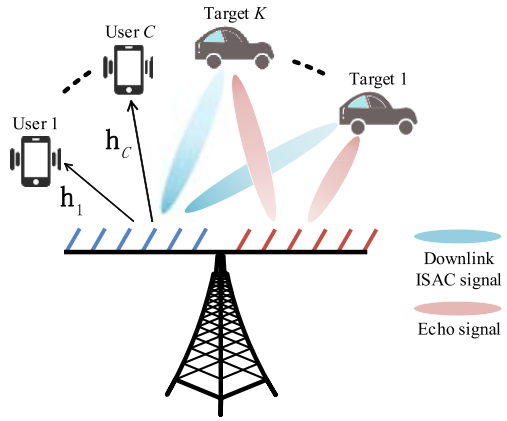

Fig. 1. Illustration of the ISAC scenario where the BS serves C downlink communication users while detecting K targets.

a bisection search algorithm. This method provides a flexible tradeoff between the multitarget sensing and multiuser communication performance, while meeting specific sensing and communication requirements and their respective priorities.

3) Finally, numerical simulations demonstrate the following: a) the necessity of transmitting additional radar signals to provide sufficient DoFs for effectively resolving multiple targets, particularly when the number of targets surpasses the number of users and b) the adoption of the constrained sensing MI upper bound as the performance metric for multitarget sensing offers an enhanced tradeoff between the sensing and communication performance. Moreover, it also significantly improves resolution for closely located multiple targets and enhances accuracy in angle estimation.

The remainder of this article is organized as follows. Section II introduces the system model along with the performance metric for multiuser communications. Section III derives the sensing MI and its tight upper bound for multitarget sensing. Section IV investigates the multiobjective optimization for ISAC beamforming, where we employ a max-min utility function method to solve the MOOP. Simulation results are presented in Section V. Finally, we provide the concluding remarks in Section VI.

Notations: Boldface lowercase and uppercase letters denote the vectors and matrices, respectively. The set of complex number is $\mathbb{C}$. The transpose, conjugate transpose, conjugate, inverse, and pseudo-inverse operation is denoted by $(\cdot)^{\mathrm{T}}$, $(\cdot)^H$, $(\cdot)^*$, $(\cdot)^{-1}$, and $(\cdot)^\dagger$, respectively. The expected value of a random argument is denoted by $\mathbb{E}(\cdot)$. We let $\otimes$ denote the Kronecker product and let $\mathbf{I}_M$ denote the M-dimensional identity matrix. The curled inequality symbol $\succeq$ is utilized to denote the generalized matrix inequality, i.e., $\mathbf{A} \succeq \mathbf{0}$ means that $\mathbf{A}$ is the positive semi-definite matrix. The symbols $\det(\cdot)$ and $\mathrm{tr}(\cdot)$ denote the determinant and trace of a matrix, respectively.

II. System Model

We consider a colocated ISAC system as shown in Fig. 1, where the BS is equipped with N_t transmit antennas and N_r receive antennas as the uniform linear arrays (ULAs). The BS aims to serve the C downlink single-antenna users while detecting the K targets. The set of communication users is indexed by $\mathcal{C} = \{1, 2, \ldots, C\}$. To achieve the satisfactory performance of communication and radar sensing, we exploit the maximum DoFs provided by MIMO and transmit M additional probing streams. The transmit signal is a sum of precoded communication signals and radar probing signals [12], [13], [18], i.e.,

$$\mathbf{X} = \mathbf{W}_c\mathbf{S}_c + \mathbf{W}_r\mathbf{S}_r \tag{1}$$

where $\mathbf{X} \in \mathbb{C}^{N_t \times L}$ is the transmit signal matrix with $L > N_t$ being the length of the signals. The ith data stream of the communication is denoted by $\mathbf{s}_i \quad \forall i \in \mathcal{C}$, and $\mathbf{S}_c = [\mathbf{s}_1^{\mathrm{T}}, \ldots, \mathbf{s}_C^{\mathrm{T}}]^{\mathrm{T}} \in \mathbb{C}^{C \times L}$ contains the C data streams intended for the C users. Similarly, the mth probing stream of radar sensing is denoted by $\mathbf{s}_{C+m}$, $m \in \{1, 2, \ldots, M\}$, and $\mathbf{S}_r = [\mathbf{s}_{C+1}^{\mathrm{T}}, \ldots, \mathbf{s}_{C+M}^{\mathrm{T}}]^{\mathrm{T}} \in \mathbb{C}^{M \times L}$ contains M individual probing streams with $M < N_t - C$ [18]. The matrices $\mathbf{W}_c = [\mathbf{w}_1, \ldots, \mathbf{w}_C] \in \mathbb{C}^{N_t \times C}$ and $\mathbf{W}_r = [\mathbf{w}_{C+1}, \ldots, \mathbf{w}_{C+M}] \in \mathbb{C}^{N_t \times M}$ contain the transmit beamforming vectors for the data streams and the probing streams, respectively.

We assume that both the communication signals and radar probing signals are wide-sense stationary stochastic processes with zero-mean and unit power [13]. The communication data signals for different users are uncorrelated, so $(1/L)\mathbb{E}[\mathbf{S}_c\mathbf{S}_c^H] = \mathbf{I}_C$. The radar probing signals are pseudo-random sequences with zero-mean and unit variance, and are uncorrelated with each other [30], i.e., $(1/L)\mathbb{E}[\mathbf{S}_r\mathbf{S}_r^H] = \mathbf{I}_M$. The communication signals and radar probing signals are assumed to be uncorrelated, namely $\mathbb{E}[\mathbf{S}_c\mathbf{S}_r^H] = \mathbf{0}$. Then, we can derive the covariance matrix of the transmit signal, given by

$$\mathbf{R}_X = \frac{1}{L}\mathbb{E}\big[\mathbf{X}\mathbf{X}^H\big] = \sum_{n=1}^{C+M} \mathbf{w}_n\mathbf{w}_n^H. \tag{2}$$

In the following, we describe the received signal model and the performance metric for multiuser communications in Section II-A. Subsequently, we present the receive signal model for the radar sensing at the BS in Section II-B.

A. Multiuser Communication Model

For downlink communications, the signal received at the ith user is expressed as

$$\mathbf{y}_i = \mathbf{h}_i^H\mathbf{X} + \mathbf{z}_i \tag{3}$$

where $\mathbf{h}_i \in \mathbb{C}^{N_t \times 1}$ is the channel matrix between the BS and the ith user, and $\mathbf{z}_i \sim \mathcal{CN}(0, \sigma_i^2\mathbf{I}_L)$ is a complex additive white Gaussian noise (AWGN) vector with zero-mean and covariance $\sigma_i^2\mathbf{I}_L$.

Since, the communication users have no prior information about the probing streams, the users suffer from the interference caused by the probing streams and the multiuser interference [13], [18]. Specifically, the received signal (3) can be rewritten as

$$\mathbf{y}_i = \mathbf{h}_i^H\mathbf{w}_i\mathbf{s}_i + \sum_{j=1, j\neq i}^{C} \mathbf{h}_i^H\mathbf{w}_j\mathbf{s}_j + \sum_{j=C+1}^{C+M} \mathbf{h}_i^H\mathbf{w}_j\mathbf{s}_j + \mathbf{z}_i \quad \forall i \in \mathcal{C}$$

(4)

where the initial term is the useful signal, while the second term denotes the interference caused by the other communication users. The third term indicates the interference originating from the radar probing signals. Thus, the SINR of the ith user is

$$\gamma_i = \frac{\left|\mathbf{h}_i^H \mathbf{w}_i\right|^2}{\sum_{j=1, j\neq i}^{C} \left|\mathbf{h}_i^H \mathbf{w}_j\right|^2 + \sum_{j=C+1}^{C+M} \left|\mathbf{h}_i^H \mathbf{w}_j\right|^2 + \sigma_i^2}. \tag{5}$$

The overall performance of the multiuser multiple-input and multiple-output (MU-MIMO) communication is evaluated by the average rate, which is given by [31]

$$r_c = \frac{1}{C}\left(\sum_{i=1}^{C} \log(1+\gamma_i)\right). \tag{6}$$

B. Radar Sensing Model

The BS uses the reflected echoes to recover the parameters of the targets. In this article, we focus on the beamforming in the spatial domain. For brevity, the sensing targets are modeled to be stationary and are located at the same range resolution as assumed in [11], [18], and [32]. With these assumptions, the target response matrix is expressed as the superposition of the response of the individual target [33], i.e.,

$$\mathbf{G} = \sum_{k=1}^{K} \beta_k \ \mathbf{b}(\theta_k) \ \mathbf{a}^H(\theta_k) \tag{7}$$

where $\mathbf{a}(\theta_k) = [1, e^{j(2\pi/\lambda)d\sin(\theta_k)}, \ldots, e^{j(2\pi/\lambda)(N_t-1)d\sin(\theta_k)}]^{\mathrm{T}} \in \mathbb{C}^{N_t\times 1}$ and $\mathbf{b}(\theta_k) = [1, e^{j(2\pi/\lambda)d\sin(\theta_k)}, \ldots, e^{j(2\pi/\lambda)(N_r-1)d\sin(\theta_k)}]^{\mathrm{T}} \in \mathbb{C}^{N_r\times 1}$ are the corresponding transmit and receive steering vectors of the echo with the direction at θ_k, respectively. In general, the target can be modeled as being composed of an infinite number of random, isotropic, and independent scatterers over the area of interest, and the complex gain of each scatterer can be modeled as a zero-mean and white complex random variable [34]. Together with the fact that the incident angles between different targets are independently distributed [35], the complex coefficients of different targets can be assumed to be independently Gaussian distributed, i.e., $\beta_k \sim \mathcal{CN}(0, \sigma_k^2) \ \ \forall k$ [36].

The distance of adjacent antenna elements is denoted by d and λ denotes the wavelength. Thus, the signal received at the BS is given by

$$\mathbf{Y}_r = \mathbf{G}\mathbf{X} + \mathbf{Z}_r \tag{8}$$

where $\mathbf{Z}_r \in \mathbb{C}^{N_r\times L}$ is a complex AWGN matrix with zero-mean and covariance $\sigma_r^2\mathbf{I}_L$.

Upon vectorizing (8), the received signal is recast as

$$\tilde{\mathbf{y}}_r = \tilde{\mathbf{X}}\tilde{\mathbf{g}} + \tilde{\mathbf{z}}_r \tag{9}$$

where $\tilde{\mathbf{y}}_r \triangleq \mathrm{vec}(\mathbf{Y}_r)$, $\tilde{\mathbf{X}} \triangleq (\mathbf{X}^{\mathrm{T}} \otimes \mathbf{I}_{N_r})$, $\tilde{\mathbf{g}} \triangleq \mathrm{vec}(\mathbf{G})$, and $\tilde{\mathbf{z}}_r \triangleq \mathrm{vec}(\mathbf{Z}_r)$. Let $\mathbf{R}_G = \mathbb{E}[\tilde{\mathbf{g}}\tilde{\mathbf{g}}^H]$ be the spatial correlation matrix of $\mathbf{G}$ and $\mathbf{R}_Z = \mathbb{E}[\tilde{\mathbf{z}}_r\tilde{\mathbf{z}}_r^H]$ be the covariance matrix of $\tilde{\mathbf{z}}_r$. To facilitate the derivation, we assume $\tilde{\mathbf{g}} \sim \mathcal{CN}(\mathbf{0}, \mathbf{R}_G)$, which is consistent with the classic literature on the radar MI [22], [23], [37]. Then, we have $\tilde{\mathbf{z}}_r \sim \mathcal{CN}(\mathbf{0}, \mathbf{R}_Z)$ and $\tilde{\mathbf{y}}_r \sim \mathcal{CN}(\mathbf{0}, \tilde{\mathbf{X}}\mathbf{R}_G\tilde{\mathbf{X}}^H + \mathbf{R}_Z)$. The covariance matrix $\mathbf{R}_G$ is given by

$$\mathbf{R}_G = \mathbb{E}\left[\tilde{\mathbf{g}}\tilde{\mathbf{g}}^H\right] \overset{(a)}{=} \sum_{k=1}^{K} \sigma_k^2 \left(\mathbf{a}^*(\theta_k) \otimes \mathbf{b}(\theta_k)\right)\left(\mathbf{a}^*(\theta_k) \otimes \mathbf{b}(\theta_k)\right)^H \tag{10}$$

where (a) follows $\mathrm{vec}(\mathbf{b}\mathbf{a}^{\mathbf{H}}) = (\mathbf{a}^* \otimes \mathbf{b})$.

To demonstrate the necessity of transmitting additional radar signals, we consider a scenario where only C communication signals are transmitted, i.e., $\mathbf{X} = \mathbf{W}_c\mathbf{S}_c$. In this case, the number of DoFs for transmit bemaforming design is limited by the number of communication users due to the fact that $\mathrm{rank}(\mathbf{R}_X) = C$. However, when there exists the K targets with $K > C$, the number of available DoFs is insufficient for accurate estimation of the targets using the angle estimation techniques, such as multiple signal classification (MUSIC) and Capon [29]. Consequently, this leads to an inevitable degradation in the performance of multitarget sensing due to the lack of radar DoFs [18]. Therefore, it is imperative to transmit additional radar signals in scenarios with a large number of targets. The detailed analysis is provided in Section V.

III. Mutual Information for Radar Sensing

In order to characterize the performance of multitarget sensing, we introduce the sensing MI which can be employed to measure how much environmental information can be observed in the BS [22]. The sensing MI is generally defined as the conditional MI between the sensing channel $\tilde{\mathbf{g}}$ and the received signal $\tilde{\mathbf{y}}_r$ with the given transmit signal [16]. Following [38], we obtain the general expression of sensing MI as:

$$\begin{aligned} I\left(\tilde{\mathbf{y}}_r; \tilde{\mathbf{g}}\middle|\tilde{\mathbf{X}}\right) &= \log\left[\det\left(\tilde{\mathbf{X}}\mathbf{R}_G\tilde{\mathbf{X}}^H + \mathbf{R}_Z\right)\right] - \log[\det(\mathbf{R}_Z)] \\ &= \log\left[\det\left(\mathbf{I} + \tilde{\mathbf{X}}\mathbf{R}_G\tilde{\mathbf{X}}^H\mathbf{R}_Z^{-1}\right)\right] \\ &\overset{(a)}{=} \log\left[\det\left(\mathbf{I} + \frac{1}{\sigma_r^2}\mathbf{R}_G\tilde{\mathbf{X}}^H\tilde{\mathbf{X}}\right)\right] \end{aligned} \tag{11}$$

where $\mathbf{R}_z$ is the covariance matrix of $\tilde{\mathbf{z}}_r$ and (a) follows the Sylvester's determinant theorem, i.e., $\det(\mathbf{I} + \mathbf{AB}) = \det(\mathbf{I} + \mathbf{BA})$. Due to the fact that the columns of the noise $\mathbf{Z}_r$ are independent of each other, we have $\mathbf{R}_Z = \sigma_r^2\mathbf{I}_{LN_r}$.

Substituting the specific expression of $\tilde{\mathbf{X}}$ into (12), the sensing MI can be rewritten as

$$\begin{aligned} I\left(\tilde{\mathbf{y}}_r; \tilde{\mathbf{g}}\middle|\tilde{\mathbf{X}}\right) &= \log\left[\det\left(\mathbf{I} + \frac{1}{\sigma_r^2}\mathbf{R}_G\left(\mathbf{X}^{\mathrm{T}} \otimes \mathbf{I}_{N_r}\right)^H\left(\mathbf{X}^{\mathrm{T}} \otimes \mathbf{I}_{N_r}\right)\right)\right] \\ &\overset{(a)}{=} \log\left[\det\left(\mathbf{I} + \frac{1}{\sigma_r^2}(\mathbf{X}^*\mathbf{X}^{\mathrm{T}} \otimes \mathbf{I}_{N_r})\mathbf{R}_G\right)\right] \end{aligned} \tag{12}$$

where (a) is based on the property of the Kronecker product $(\mathbf{AB})\otimes(\mathbf{CD}) = (\mathbf{A}\otimes\mathbf{C})(\mathbf{B}\otimes\mathbf{D})$ and $\det(\mathbf{I}+\mathbf{AB}) = \det(\mathbf{I}+\mathbf{BA})$. However, the expression of sensing MI in (12) is intractable due to the Kronecker product structure. Therefore, we recast the sensing MI into a more concise and intuitive form in Lemma 1.

Lemma 1: By performing mathematical transformations, we obtain a novel form of sensing MI, namely

$$I\left(\tilde{\mathbf{y}}_r;\tilde{\mathbf{g}}\middle|\tilde{\mathbf{X}}\right)=\log\left[\det(\Phi+\Lambda)\prod_{k=1}^{K}\sigma_k^2\right] \tag{13}$$

where the positive semi-definite matrix $\Phi\in\mathbb{C}^{K\times K}$ and diagonal matrix $\Lambda\in\mathbb{C}^{K\times K}$ are, respectively, defined by

$$\begin{aligned}[\Phi]_{i,j}&\triangleq\frac{L}{\sigma_r^2}\mathrm{tr}\left(\mathbf{A}^H(\theta_i)\mathbf{A}(\theta_j)\mathbf{R}_X\right)\\&=\frac{\alpha_{ij}L}{\sigma_r^2}\mathbf{a}^H(\theta_i)\left(\sum_{n=1}^{C+M}\mathbf{w}_n\mathbf{w}_n^H\right)\mathbf{a}(\theta_j)\end{aligned} \tag{14}$$

and

$$\Lambda\triangleq\mathrm{diag}\left\{\frac{1}{\sigma_1^2},\frac{1}{\sigma_2^2},\ldots,\frac{1}{\sigma_K^2}\right\} \tag{15}$$

where $[\Phi]_{i,j}$ is the (i,j)th element of Φ, $\mathbf{A}(\theta_k)\triangleq\mathbf{b}(\theta_k)\mathbf{a}^H(\theta_k)$, and $\alpha_{ij}\triangleq\mathbf{b}^H(\theta_i)\mathbf{b}(\theta_j)$.

Proof: Refer to Appendix A. ■

It is noted that the elements of Φ in (14) are the cross-correlation between the signals reflected back from the targets of interest, defined as the cross-correlation pattern [39]. Therefore, (13) indicates that the multitarget sensing MI relies on the statistical characteristics of the reflection coefficients $\beta_k\ \ \forall k$ and the cross-correlation pattern among the signals. However, (13) is still complex and intractable due to the coupling of each element in Φ via the beamforming vectors. To simplify the expression and obtain the structural features of the maximum sensing MI, we derive an upper bound of sensing MI as shown below.

Theorem 1: The upper bound of sensing MI is denoted by I_{up}, and we have

$$I_{\mathrm{up}}=\sum_{\mathrm{k}=1}^{K}\log\left(1+\frac{N_r\sigma_k^2L}{\sigma_r^2}\mathbf{a}^H(\theta_k)\left(\sum_{n=1}^{C+M}\mathbf{w}_n\mathbf{w}_n^H\right)\mathbf{a}(\theta_k)\right). \tag{16}$$

The bound is tight when

$$\mathbf{a}^H(\theta_j)\left(\sum_{n=1}^{C+M}\mathbf{w}_n\mathbf{w}_n^H\right)\mathbf{a}(\theta_i)=0\ \ \forall i,j(i\neq j) \tag{17}$$

where $\alpha_{ji}=\mathbf{b}^H(\theta_j)\mathbf{b}(\theta_i)$.

Proof: Based on Lemma 1, applying the Hadamard's inequality [40, Sec. 6.1] for the determinant of an $N\times N$ positive semi-definite matrix to (13), we obtain that

$$\begin{aligned}&\log\left[\det(\Phi+\Lambda)\prod_{k=1}^{K}\sigma_k^2\right]\\&\leq\log\left[\prod_{i=1}^{K}\left(1+\frac{\alpha_{ii}\sigma_i^2L}{\sigma_r^2}\mathbf{a}^H(\theta_i)\left(\sum_{n=1}^{C+M}\mathbf{w}_n\mathbf{w}_n^H\right)\mathbf{a}(\theta_i)\right)\right]\end{aligned} \tag{18}$$

with the equality holding if and only if $\Phi+\Lambda$ is diagonal, i.e.,

$$\mathbf{a}^H(\theta_j)\left(\sum_{n=1}^{C+M}\mathbf{w}_n\mathbf{w}_n^H\right)\mathbf{a}(\theta_i)=0\ (i\neq j). \tag{19}$$

Substituting $\alpha_{i,i}=N_r$ into the right-hand side of (18), we can obtain the upper bound of sensing MI in (16). ■

Equation (17) represents the zero-forced cross-correlation constraints, indicating that the signals reflected from different targets are independent of each other. When these constraints are satisfied, the upper bound of sensing MI can be achieved. However, fully eliminating the cross-correlation pattern is highly challenging. In practical applications, it is often approximated by imposing constraints to ensure that the absolute value of cross-correlation pattern is smaller than a sufficiently low threshold value [36], namely

$$\left|\mathbf{a}^H(\theta_j)\left(\sum_{n=1}^{C+M}\mathbf{w}_n\mathbf{w}_n^H\right)\mathbf{a}(\theta_i)\right|\leq\kappa,\ (i\neq j) \tag{20}$$

where $\kappa\to 0$.

Additionally, we see that the second term in (16) is the SINR of the reflected echo from the kth target, which is denoted by

$$\mathrm{SINR}_k=\frac{N_r\sigma_k^2L}{\sigma_r^2}\mathbf{a}^H(\theta_k)\left(\sum_{n=1}^{C+M}\mathbf{w}_n\mathbf{w}_n^H\right)\mathbf{a}(\theta_k). \tag{21}$$

By substituting (21) into (16), we have the following insight given in Corollary 1.

Corollary 1: The upper bound of sensing MI can be expressed in a form similar to the communication sum-rate, i.e.,

$$I_{\mathrm{up}}=\sum_{\mathrm{k}=1}^{K}\log(1+\mathrm{SINR}_k) \tag{22}$$

where the component $\log(1+\mathrm{SINR}_k)$ in I_{up} represents the sensing MI solely focused on the kth target. Therefore, the upper bound of the multitarget sensing MI can be regarded as the sum of the individual single-target sensing MI.

As mentioned in [29] and [39], the statistical performance of adaptive MIMO radar heavily relies on the cross-correlation pattern. It also indicates that the transmit beamforming design should aim to minimize the cross-correlation among the signals form specified target directions while optimizing the transmission power in those directions.

Following this principle, in the next section, we use the upper bound of sensing MI as the sensing performance metric to optimize the beamforming vectors, which can potentially enhance transmit power at given target directions.[1] Concurrently, we use the cross-correlation (20) to ensure the attainability of the upper bound and minimize the cross-correlation pattern.

IV. Joint Beamforming Based on Multiobjective Optimization

In this section, we investigate a general transmit beamforming method that provides a flexible tradeoff

[1]While I_{up} depends on the target directions $\theta_k\ \ \forall k$ as can be seen in (17), maximizing I_{up} can be interpreted as optimizing the beamforming vectors $\mathbf{w}$ with respect to the directions toward the potential targets. This is typical for MIMO radar systems operating in tracking mode, where the BS has knowledge of the target directions and can obtain them from the previous observations [13]. In the case of static or slowly moving targets, it is reasonable to utilize the estimated or predicted directions for the beamforming design [18].

between the multitarget sensing and multiuser communication performance. We begin by formulating a MOOP to concurrently optimize the sensing MI and the SINR of each user in Section IV-A. Then, we employ the semidefinite relaxation (SDR) to tackle the rank-one constraint in Section IV-B. To efficiently solve the complex MOOP, we propose a max-min utility optimization method to attain the Pareto boundary of the MOOP in Section IV-C, which also considers fairness among the multiple users and targets.

A. Problem Formulation

The expressions in (5) and (16) reveal that the performance of multitarget sensing and multiuser communication are coupled together through the transmit beamforming vectors, which can lead to inherent conflicts and tradeoff. To comprehensively investigate the tradeoff and optimize the performance of communication and sensing simultaneously, we introduce a MOOP framework.

Since, the maximum sensing MI is achieved by maximizing I_{up} subject to (17), we formulate the MOOP as follows:

$$\max_{\{\mathbf{w}_n\}} \ \left\{I_{\text{up}}, \gamma_1, \ldots, \gamma_C\right\} \tag{23a}$$

$$\text{s.t.} \ \ \text{tr}\left(\sum_{n=1}^{C+M} \mathbf{w}_n \mathbf{w}_n^H\right) \le P_T \tag{23b}$$

$$\mathbf{a}^H(\theta_j)\left(\sum_{n=1}^{C+M} \mathbf{w}_n \mathbf{w}_n^H\right)\mathbf{a}(\theta_i) = 0 \ \ (i \ne j) \tag{23c}$$

$$I_{\text{up}} \ge \Lambda \tag{23d}$$

$$\gamma_i \ge \Gamma_i \ \forall i \in \mathcal{C} \tag{23e}$$

where P_T is the total transmit power of the BS. $\Lambda \ge 0$ and $\Gamma_i \ge 0$ indicate the lowest acceptable level of the sensing MI and SINR of the ith user, respectively. Constraint (23b) ensures that the total transmit power remains within a predetermined limit, while (23c) guarantees that the sensing MI enables to achieve its upper bound. The MOOP (23) is nonconvex due to its quadratic terms in both the objective functions and constraints, making it difficult to solve directly. Nevertheless, we show in Section IV-B that it can be reformulated into a more tractable relaxed problem using SDR. In Section IV-C, we propose a max-min utility optimization method to obtain a specific Pareto optimal solution for the relaxed MOOP. Furthermore, we prove that this Pareto optimal solution for the relaxed MOOP also serves as the Pareto optimizer for the original MOOP (23), i.e., the relaxation is tight.

B. Problem Transformation Via Semidefinite Relaxation

In this section, we employ the SDR strategy to tackle the nonconvex problem (23). To this end, we first introduce variables $\mathbf{R}_n = \mathbf{w}_n \mathbf{w}_n^H \succeq \mathbf{0}$ with $\text{rank}(\mathbf{R}_n) = 1$, where $n = 1, \ldots, C+M$. Subsequently, by substituting $\{\mathbf{R}_n\}$ into (5), (16), (23b), and (23c), we can linearize the quadratic terms in (23). Thus, the expressions in (5) and (16) are rewritten as

$$\gamma_i = \frac{\mathbf{h}_i^H \mathbf{R}_i \mathbf{h}_i}{\sum_{n=1, n\ne i}^{C} \mathbf{h}_i^H \mathbf{R}_n \mathbf{h}_i + \sum_{n=C+1}^{C+M} \mathbf{h}_i^H \mathbf{R}_n \mathbf{h}_i + \sigma_c^2} \ \ \forall i \in \mathcal{C} \tag{24}$$

$$I_{\text{up}} = \sum_{k=1}^{K} \log\left(1 + \frac{N_r \sigma_k^2 L}{\sigma_r^2} \mathbf{a}^H(\theta_k)\left(\sum_{n=1}^{C+M} \mathbf{R}_n\right)\mathbf{a}(\theta_k)\right). \tag{25}$$

Then, (23b) and (23c) are rewritten as

$$\text{tr}\left(\sum_{n=1}^{C+M} \mathbf{R}_n\right) \le P_T \tag{26a}$$

$$\text{tr}\left(\mathbf{a}(\theta_i)\mathbf{a}^H(\theta_j)\left(\sum_{n=1}^{C+M} \mathbf{R}_n\right)\right) = 0 \ \ (i \ne j). \tag{26b}$$

With the newly derived objective functions and constraints, the MOOP (23) is reformulated as

$$\max_{\{\mathbf{R}_n\}} \ \left\{I_{\text{up}}, \gamma_1, \ldots, \gamma_C\right\} \tag{27a}$$

$$\text{s.t.} \ \ \text{tr}\left(\sum_{n=1}^{C+M} \mathbf{R}_n\right) \le P_T \tag{27b}$$

$$\text{tr}\left(\mathbf{a}(\theta_i)\mathbf{a}^H(\theta_j)\left(\sum_{n=1}^{C+M} \mathbf{R}_n\right)\right) = 0 \ \ (i \ne j) \tag{27c}$$

$$\mathbf{R}_n \succeq 0 \ \ \forall n \tag{27d}$$

$$\text{rank}(\mathbf{R}_n) = 1 \ \ \forall n \tag{27e}$$

$$\text{(23d) and (23e).} \tag{27f}$$

Since, the rank-one constraints (27e) are nonconvex in (27), we use the SDR strategy to tackle it. Omitting the rank-one constraints leads to the following relaxation:

$$\max_{\{\mathbf{R}_n\}} \ \left\{I_{\text{up}}, \gamma_1, \ldots, \gamma_C\right\} \tag{28a}$$

$$\text{s.t.} \ \ \text{(23d), (23e), (27b), (27c), and (27d).} \tag{28b}$$

The MOOP (28) aims to find a transmit strategy $\{\mathbf{R}_n\}$ that satisfies transmit power and cross-correlation constraints while maximizing the sensing performance I_{up} and communication performance $\gamma_1, \ldots, \gamma_C$ for all the users. Nevertheless, the conflict arises between maximizing $\gamma_1, \ldots, \gamma_C$ and I_{up}, as they are coupled through the transmit strategy $\{\mathbf{R}_n\}$. Typically, there does not exist a singular transmit strategy that can simultaneously optimize all these objectives. Therefore, it is instructive to consider the set of feasible performance outcomes for all the feasible transmit strategies, i.e., the achievable performance region of the multitarget and multiuser ISAC system. The achievable performance region $\mathcal{M} \subset \mathbb{R}_+^{C+1}$ is defined as a set of achievable performance pairs with all the feasible transmit strategies

$$\mathcal{M} = \left\{\left(I_{\text{up}}, \gamma_1, \ldots, \gamma_C\right) : \forall\{\mathbf{R}_1, \ldots, \mathbf{R}_{C+M}\} \in \mathcal{R}\right\} \tag{29}$$

where $\mathcal{R}$ is the feasible transmit strategy set with the transmit power and zero-forced cross-correlation constraints

$$\mathcal{R} = \left\{(\mathbf{R}_1, \ldots, \mathbf{R}_{C+M}) : \mathbf{R}_n \succeq 0 \ \ \forall n, \text{tr}\left(\sum_{n=1}^{C+M} \mathbf{R}_n\right) \le P_T \right.$$
$$\left. \text{tr}\left(\mathbf{a}(\theta_i)\mathbf{a}^H(\theta_j)\left(\sum_{n=1}^{C+M} \mathbf{R}_n\right)\right) = 0 \ \ (i \ne j)\right\}. \tag{30}$$

The region describes the achievable sensing MI and communication SINRs that can be simultaneously attained under transmit power and the zero-forced cross-correlation constraints. Typically, we seek to obtain a set of optimal solutions for MOOP, known as the Pareto optimal solutions, which are incomparable to each other and no superior solution exists in the objective space. These solutions are found on a subset of the outer boundary of $\mathcal{M}$ referred to as the Pareto boundary, where an improvement in a single performance implies a degradation in the other performances:

Definition 1: The *Pareto boundary* $\partial\mathcal{M} \subseteq \mathcal{M}$ consists of all $\mathbf{x} \in \mathcal{M}$ for which there is no $\mathbf{x}' \in \mathcal{M}\backslash\{\mathbf{x}\}$ with $\mathbf{x}' \geq \mathbf{x}$ [41, Definition 4].

C. Max-Min Utility Optimization

We next provide the algorithm to obtain the Pareto optimal solutions for the MOOP (28). A common approach to address the MOOP is to combine multiple objective functions into a system utility function, denoted by $H(\cdot)$. In order to meet the minimum communication and sensing performance thresholds and account for fairness between the multitarget sensing performance and multiuser communication performance, we employ the minimum weighted compromise function as the system utility function [41], [42]. For a given feasible operating point $\mathbf{x} = (I_{\text{up}}, \gamma_1, \ldots, \gamma_C) \in \mathcal{M}$, the system utility function is given by

$$H(\mathbf{x}) = \min_i \left\{ \frac{I_{\text{up}} - \Lambda}{\alpha}, \frac{\gamma_i - \Gamma_i}{\omega_i} \right\} \tag{31}$$

where the communication and sensing performance should be in excess of the lowest acceptable levels, i.e., $I_{\text{up}} \geq \Lambda$ and $\gamma_i \geq \Gamma_i \quad \forall i \in \mathcal{C}$. The parameters $\alpha \in \mathbb{R}_+$ and $\omega_i \in \mathbb{R}_+$ are the weights of sensing and the ith communication user, respectively, which satisfy $\sum_{i=1}^{C} \omega_i + \alpha = 1$. Next, we demonstrate that a set of Pareto solutions for the MOOP (28) can be obtained by solving the following system function optimization problem:

$$\max_{\{\mathbf{R}_n\}} \ \min_i \left\{ \frac{I_{\text{up}} - \Lambda}{\alpha}, \frac{\gamma_i - \Gamma_i}{\omega_i} \right\} \tag{32a}$$

$$\text{s.t.} \ \ (23\text{d}), (23\text{e}), (27\text{b}), (27\text{c}), \ \text{and} \ \ (27\text{d}). \tag{32b}$$

It is worth noting that the objective function in (32) can provide a flexible tradeoff between sensing and communication by assigning appropriate weights. For instance, in two extreme weight configuration cases, (32) can be transformed into the sensing MI optimization problem with the SINR constraints (denoted by Case 1) and the SINR optimization problem with the sensing MI constraint (denoted by Case 2), as follows.

Case 1: In this case, we set $\Lambda = 0$, $\alpha = 1$, and $\omega_i \to 0$, which gives higher priority to sensing over communication. The problem (32) is transformed into an optimization problem that maximizes the sensing MI while satisfying each user's SINR constraint

$$\max_{\{\mathbf{R}_n\}} \ \{I_{\text{up}}\} \tag{33a}$$

$$\text{s.t.} \ \ (23\text{e}), (27\text{b}), (27\text{c}), \ \text{and} \ \ (27\text{d}). \tag{33b}$$

Case 2: In this case, we set $\Gamma_i = 0$, $\omega_i = 1/C$, and $\alpha \to 0$, which gives higher priority to communication. Additionally, every user is considered to have the same importance. As a result, (32) reduces to a maximization of the minimum SINR subject to the sensing MI constraint

$$\max_{\{\mathbf{R}_n\}} \min_i \ \{\gamma_i\} \tag{34a}$$

$$\text{s.t.} \ \ (23\text{d}), (27\text{b}), (27\text{c}), \ \text{and} \ \ (27\text{d}). \tag{34b}$$

However, the achievable performance region $\mathcal{M}$ is typically nonconvex, which poses a challenge in obtaining the Pareto solutions for the MOOP (28). For instance, if $\mathcal{M}$ is a nonnormal set with internal holes, it can lead to a complex and challenging resolution of the Pareto boundary [41]. Given this, we first investigate the properties of $\mathcal{M}$ to demonstrate its compactness and normality, and consequently demonstrate that the Pareto solutions for (28) can be attained by solving the system function optimization (32).

Definition 2: $\mathcal{M} \subset \mathbb{R}_+^n$ is called a compact set if it is closed and bounded [14, Definition 2].

Definition 3: $\mathcal{M} \subset \mathbb{R}_+^n$ is called a normal set if for any point $\mathbf{x} \in \mathcal{M}$, all $\mathbf{x}' \in \mathbb{R}_+^n$ with $\mathbf{x}' \leq \mathbf{x}$ (component-wise inequalities) also satisfy $\mathbf{x}' \in \mathcal{M}$ [42, Definition 4].

Lemma 2: The performance region $\mathcal{M}$ is a compact and normal set.

Proof: Please refer to Appendix B. ■

Additionally, we can observe from (31) that the system utility function $H(\cdot)$ is strictly increasing. Combining this with the characterization of $\mathcal{M}$ as a compact and normal set, we can derive the following important conclusion.

Lemma 3: If $H(\cdot)$ is a strictly increasing function and $\mathcal{M}$ is a compact and normal set, the global optimum to $\max_{\mathbf{x}\in\mathcal{M}} H(\mathbf{x})$ is attained on $\partial\mathcal{M}$.

Proof: Refer to [42, Lemma 2]. ■

Based on Lemma 3, we can attain the Pareto boundary of MOOP (28) by solving (32).

We next present the algorithm to solve (32). Specifically, letting

$$r = \min_i \left\{ \frac{I_{\text{up}} - \Lambda}{\alpha}, \frac{\gamma_i - \Gamma_i}{\omega_i} \right\} \tag{35}$$

the max-min utility (32) can be recast as

$$\max_{\{\mathbf{R}_n\}} \quad r \tag{36a}$$

$$\text{s.t.} \ \ I_{\text{up}} \geq \Lambda + \alpha r \tag{36b}$$

$$\gamma_i \geq \Gamma_i + \omega_i r \quad \forall i \in \mathcal{C} \tag{36c}$$

$$(27\text{b}), (27\text{c}), \ \text{and} \ \ (27\text{d}). \tag{36d}$$

We observe that (36) has a geometric interpretation, where we can find the optimal point in the Pareto boundary $\partial\mathcal{M}$ by starting from an initial point $\mathbf{x} = (\Lambda, \Gamma_1, \ldots, \Gamma_C,) \in \mathcal{M}$ determined by the performance thresholds and following a ray in the direction of $\mathbf{c} = [\alpha, \omega_1, \ldots, \omega_C]^{\text{T}}$ determined by the sensing and communication weights. Since, $\mathcal{M}$ is a compact and normal set, the ray intersects the Pareto boundary at an unique point. For the fixed weights $\alpha, \omega_1, \ldots, \omega_C$, we first define an upper bound of r denoted by $r_{\max}$, where $\mathbf{x} + \mathbf{c}r_{\max}$ is outside $\mathcal{M}$. The initial upper bound for r can be chosen as

Algorithm 1 Bisection Search to Attain the Pareto Boundary

Initialize Λ, α, $\{\Gamma_i\}$, $\{\omega_i\}$, $r_{\min}$, $r_{\max}$, $r^{(1)} = (r_{\min} + r_{\max})/2$, the tolerance ε, and set $j = 1$.
repeat
  if the problem (37) is feasible for $r^{(j)}$ **then**
    $r_{\min} = r^{(j)}$;
  else
    $r_{\max} = r^{(j)}$;
  end if
  Update $j := j + 1$;
  Update $r^{(j)} := [r_{\min} + r_{\max}]/2$;
until $\left|r^{(j)} - r^{(j-1)}\right| \le \varepsilon$;
Solve the feasible problem (37) for $r^{(j)}$.
Output the optimal solution $\{\mathbf{R}_1, \ldots, \mathbf{R}_{C+M}\}$.

a sufficiently large number, or it can be computed as $r_{\max} = \sum_{i=1}^{C} (P_T \omega_i \|h_i\|^2/\sigma_i^2) + \alpha \sum_{k=1}^{K} \log(1 + [P_T N_t^2 \sigma_k^2 L/\sigma_r^2])$. The optimal value of (36) lies on the line segment $[0, r_{\max}]$.

Therefore, (36) can be solved by performing bisection search on the range $[0, r_{\max}]$, which decomposes it into a series of feasible subproblems. That is, for a given $r \ge 0$, we can efficiently check if there exists the feasible transmit strategies $\{\mathbf{R}_1, \ldots, \mathbf{R}_{C+M}\}$ that satisfies the constraints in (36). However, due to the nonconvex and nonlinear (36b), the feasibility problem remains computationally intractable. To tackle this issue, we further consider fairness between the multiple targets. By assigning weights ξ_k to each sensing target, where $\sum_{k=1}^{K} \xi_k = 1$, we can equivalently transform the nonconvex (36b) into a series of convex constraints. Therefore, we can achieve fairness in the sensing performance of each target and convert the feasibility problem into the following convex problem:

$$\text{find} \quad \{\mathbf{R}_1, \ldots, \mathbf{R}_{C+M}\} \tag{37a}$$

$$\text{s.t.} \quad \log(1 + \text{SINR}_k) \ge \xi_k(\Gamma + \alpha r) \quad \forall k \tag{37b}$$

$$(27b), (27c), (27d), \text{ and } (36c). \tag{37c}$$

We summarize the procedure to solve (36) in Algorithm 1. In particular, for a given convergence threshold ε, the algorithm can find an interval $[r_{\min}, r_{\max}]$ for the optimal value of (36) that satisfies $|r_{\min}, r_{\max}| \le \varepsilon$ in a limited number of iterations, which scales only with ε, i.e., $\lceil \log_2(r_{\max}/\varepsilon) \rceil$.

Specifically, when the convergence threshold ε is small enough, it is reasonable to approximate that the solution obtained by Algorithm 1 is the optimal solution of (36). The bisection search method in Algorithm 1 requires $\lceil \log_2(r_{\max}/\varepsilon) \rceil$ iterations to find an interval of length ε containing the optimal value. In each iteration, the convex feasibility (37) is solved using the interior-point methods, which has a worst-case complexity of $\mathcal{O}((C+M)^3 N_t^6 + (K^2 + C)(C+M)N_t^2)$ [43], where C, M, K, and N_t denote the number of communication users, radar streams, targets, and transmit antennas, respectively. Therefore, the overall computational complexity of Algorithm 1 is given by $\mathcal{O}(\lceil \log_2(r_{\max}/\varepsilon) \rceil \cdot ((C+M)^3 N_t^6 + (K^2 + C)(C+M)N_t^2))$, which is polynomial in the number of iterations, targets, users, radar streams, and antennas.

Based on the previous analysis, it can be concluded that the optimal solution to (36) lies on the Pareto boundary of (28). However, the optimal solution of (36) may be with high ranks, indicating that the SDR solution is not necessarily tight to (27). We introduce Theorem 2 to prove the existence of an optimal rank-one solution for (36), which corresponds to the rank-one Pareto optimal solution for (28).

Theorem 2: The problem (36) always has an optimal solution $\{\bar{\mathbf{R}}_1, \ldots, \bar{\mathbf{R}}_{C+M}\}$ that satisfies

$$\text{rank}(\bar{\mathbf{R}}_n) = 1 \quad \forall n. \tag{38}$$

Proof: Refer to Appendix C. ∎

We next introduce the construction process of the rank-one solution. According to Appendix C, when the optimal solution for (36) is obtained as $\{\mathbf{R}_1^*, \ldots, \mathbf{R}_{C+M}^*\}$, we can use it to construct a rank-one optimal solution $\{\bar{\mathbf{R}}_1, \ldots, \bar{\mathbf{R}}_{C+M}\}$ and the corresponding optimal beamforming vectors $\{\bar{\mathbf{w}}_1, \ldots, \bar{\mathbf{w}}_{C+M}\}$. First, $\{\bar{\mathbf{R}}_1, \ldots, \bar{\mathbf{R}}_C\}$ and $\{\bar{\mathbf{w}}_1, \ldots, \bar{\mathbf{w}}_C\}$ can be computed as

$$\bar{\mathbf{w}}_i = \frac{\mathbf{R}_i^* \mathbf{h}_i}{\sqrt{\mathbf{h}_i^H \mathbf{R}_i^* \mathbf{h}_i}}, \bar{\mathbf{R}}_i = \bar{\mathbf{w}}_i \bar{\mathbf{w}}_i^H \quad \forall i \in \mathcal{C}. \tag{39}$$

Then, we can obtain $\{\bar{\mathbf{w}}_{C+1}, \ldots, \bar{\mathbf{w}}_{C+M}\}$ by taking the Cholesky decomposition

$$\bar{\mathbf{W}}_r \bar{\mathbf{W}}_r^H = \sum_{n=1}^{C+M} \mathbf{R}_n^* - \sum_{i=1}^{C} \bar{\mathbf{R}}_i \tag{40}$$

where $\bar{\mathbf{W}}_r = [\bar{\mathbf{w}}_{C+1}, \ldots, \bar{\mathbf{w}}_{C+M}]$ is a lower triangular matrix. Therefore, the rank-one matrices $\{\bar{\mathbf{R}}_{C+1}, \ldots, \bar{\mathbf{R}}_{C+M}\}$ can be constructed as $\bar{\mathbf{R}}_j = \bar{\mathbf{w}}_j \bar{\mathbf{w}}_j^H$ for $j = C+1, \ldots, C+M$. Hence, $\{\bar{\mathbf{R}}_1, \ldots, \bar{\mathbf{R}}_{C+M}\}$ is a Pareto optimal solution to (27), which demonstrates that it is tight to transform (27) into (28) via SDR. Furthermore, the beamforming vectors $\{\bar{\mathbf{w}}_1, \ldots, \bar{\mathbf{w}}_{C+M}\}$ constitute a Pareto optimal solution for the original MOOP (23).

V. Simulation Results

In this section, we evaluate the performance of the proposed multiobjective optimization for the MIMO-ISAC systems through the Monte-Carlo simulation results. The communication performance is evaluated in terms of the average rate of the MU-MIMO communication defined in (6), while the sensing performance is evaluated in terms of the sensing MI. We use the following simulation settings unless specified otherwise. The BS is equipped with the $N_t = 32$ transmit antennas and $N_r = 32$ receive antennas. The length of the transmit signal is set to $L = 1024$ [13]. Both the antenna arrays are ULAs with the same antenna spacing $d = \lambda/2$. The total transmit power is $P_T = 40$ dBm. We assume that the noise power for each communication user are the same, i.e., $\sigma_i^2 = 0$ dBm $\forall i \in \mathcal{C}$ [18]. And the communication SNR of each user is defined as $\text{SNR} = (P_T/\sigma_i^2)$. We assume that the noise power in the received radar signal is $\sigma_r^2 = 0$ dBm [18]. For simplicity, the variance of the scattering coefficients are assumed to be the same, i.e., $\sigma_k^2 = \sigma^2$ $\forall k$. The radar SNR is defined as $\text{SNR}_{\text{radar}} = (|\sigma|^2 P_T/\sigma_r^2)$. Without

loss of generality, we consider the Rician fading for the communication channels. In this case, the communication channel for each user has the structure [44]

$$\mathbf{h}_i = \sqrt{\frac{\mu}{\mu+1}}\Delta + \sqrt{\frac{1}{\mu+1}}\mathbf{u} \quad \forall i \in \mathcal{C} \tag{41}$$

where $\mathbf{\Delta}$ denotes the complex Line of Sight phase vector with the nth element having the property $|\Delta_n|^2 = 1$, $\mathbf{u}$ denotes the scattered component vector with the nth element $u_n \sim \mathcal{CN}(0, 1)$, and μ is the Rician factor. Especially when $\mu = 0$, the Rician fading channel degenerates to the Rayleigh fading channel [45]. The convergence tolerance is set to $\epsilon = 0.01$.

To validate the effectiveness of our proposed beamforming design based on multiobjective optimization (labeled "proposed method"), the following schemes are considered as benchmarks.

1) *Radar-Only:* It denotes the scheme without considering communication SINR constraints, which helps evaluate the best sensing performance and serves as the performance upper bound of radar sensing.
2) *Communication-Only:* This scheme only considers the data transmission by omitting the sensing MI constraints (36b) when solving (36). This scheme can yield maximum communication performance.
3) *MI-Constrained:* This scheme only exploits the downlink communication signals for sensing and maximizes the lower bound of communications SINR under the sensing MI constraint [15].
4) *Sensing-Centric:* This scheme corresponds to Case 1, which maximizes the sensing MI while satisfying the SINR constraints for each user.
5) *Communication-Centric:* This scheme corresponds to Case 2, which maximizes the SINR for each user while satisfying the constraints of sensing MI.
6) *ZF-Violated:* This scheme maximizes the upper bound of sensing MI and the SINR for each user while neglecting the zero-forced cross-correlation constraints in (27c).

A. Convergence Performance

This section aims at analysing the convergence performance of the proposed algorithm considering different numbers of antennas. We assume that the number of receive antennas N_r is set equal to N_t. The numbers of communication users and sensing targets are $C = 2$ and $K = 2$, respectively.

Fig. 2(a) shows the sensing MI versus iteration number. It can be observed that the sensing MI increases along with the iteration monotonously for all the considered conditions. It is noted that the average number of iterations that makes the sensing MI converge is about 5. The average rate of communication versus iteration number is also depicted in Fig. 2(b). Besides, it can be observed in Fig. 2(a) and (b) that the number of iterations required in the algorithm increases with the increase of N_t, because the increase of antenna numbers enlarges the feasible set $\{\mathbf{R}_1, \ldots, \mathbf{R}_{C+M}\}$.

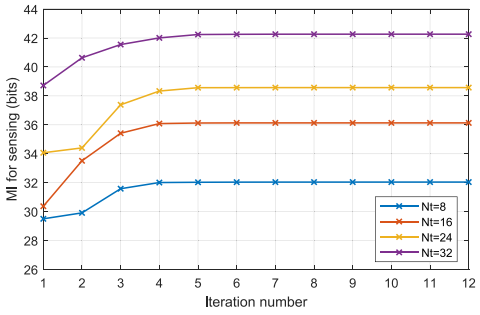

(a)

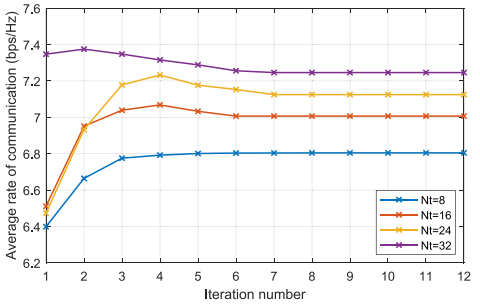

(b)

Fig. 2. Convergence of the proposed algorithm. (a) Sensing MI versus the number of iterations for $N_t = 8, 16, 24, 32$. (b) Average rate of communication versus the number of iterations for $N_t = 8, 16, 24, 32$.

B. Beampattern Performance

In this section, we show the optimized beampattern performance for different K values. We assume the $C = 2$ users at the location $\theta_{C1} = -45°$ and $\theta_{C2} = -15°$, respectively. The SINR constraint of each communication user is $\Gamma_i = 5$ dB $\forall i \in \mathcal{C}$. And the threshold of sensing MI is $\Lambda = 10$ bits. The beampatterns obtained via the mentioned schemes are depicted in Fig. 3(b) for the $K = 3$ targets located at 20°, 40°, and 60° and in Fig. 3(a) for the $K = 2$ targets located at 20° and 40°.

It can be seen from Fig. 3(b) that the proposed method has three radar mainlobes, matching the locations of the radar-only design. However, there are only two radar mainlobes located at around 20° and 40° for the MI-constrained approach. We note that the DoF for the MIMO beamforming is determined by the rank of the covariance matrix [13]. In the MI-constrained approach, only $C = 2$ communication streams are transmitted, and thus the DoF is no larger than the number of users C. If C is less than the rank of the optimal radar-only design covariance matrix, the MI-constrained approach cannot provide enough DoF to synthesize the desired radar beams, explaining the degraded beampattern observed in Fig. 3(b). The proposed method simultaneously transmits C transmission streams and M probing streams, which can provide enough DoF for the transmit beamforming, and thus can produce the beampatterns close to that of the optimal radar-only method. In Fig. 3(a), however, it is clearly observed that the proposed approach has enough DoF to generate a beampattern similar to that of the radar-only method for the $K = 2$ targets.

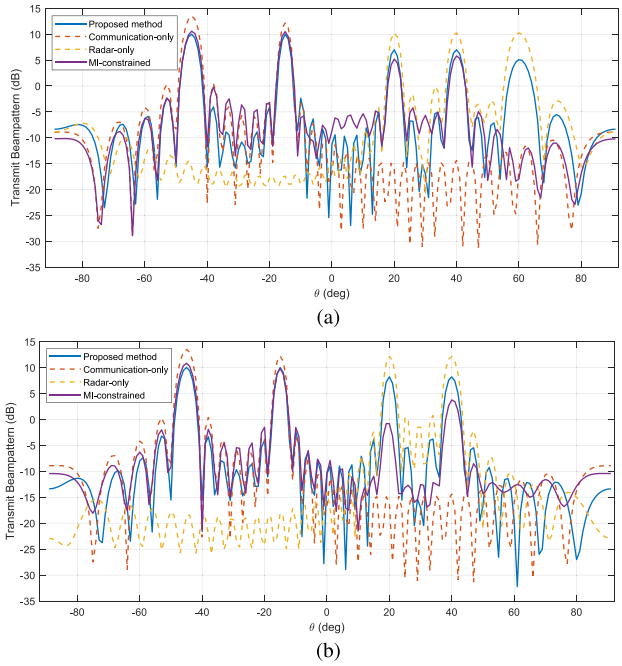

Fig. 3. Transmit beampattern for the proposed method and benchmarks. (a) Optimized transmit beampatterns with $K = 3$. (b) Optimized transmit beampatterns with $K = 2$.

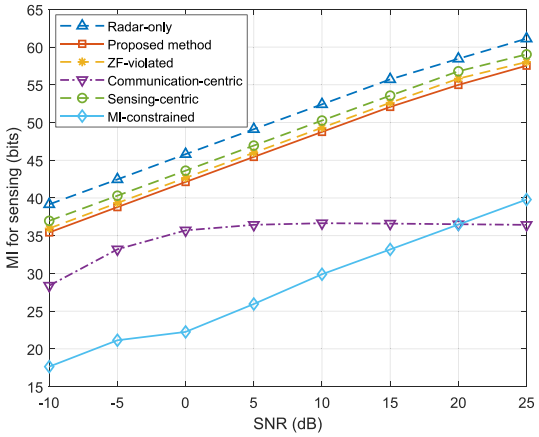

Fig. 4. Sensing MI versus receive SNR.

C. Comparisons of Communication and Sensing Performance

In Fig. 4, we show the sensing MI versus the received SNR of the echo signal for the various beamforming schemes. The numbers of communication users and sensing targets are $C = 2$ and $K = 2$, respectively. We observe that the radar-only approach achieves the highest sensing MI among the compared schemes since it is not constrained by communication performance. Subsequently, the sensing-centric scheme achieves sensing MI second only to the radar-only case, as it focuses solely on meeting the minimum communication performance requirements, with the remaining transmit power allocated toward enhancing sensing capabilities. The proposed method exhibits superior sensing MI performance over the MI-constrained and communication-centric schemes.

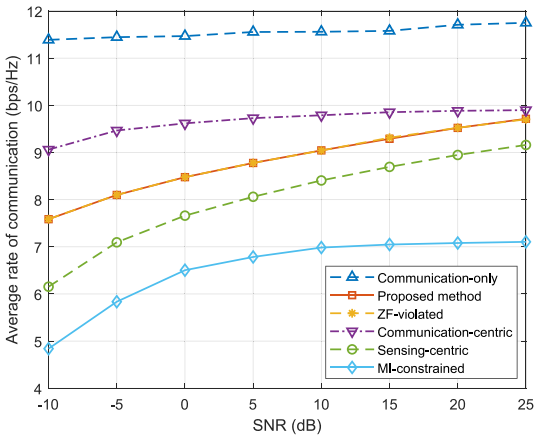

Fig. 5. Average rate of the MU-MIMO communication versus SNR.

It is also noted that the sensing MI of the communication-centric scheme increases very slowly with SNR, as this scheme solely focuses on meeting the minimum sensing MI requirement, allocating the remaining transmit power to improve the communication SINR for each user. Additionally, we observe that the proposed method closely approaches the ZF-violated scheme. This indicates that the impact of cross-correlation (27c) on the achievable maximum sensing MI is minimal. Nevertheless, in order to fully compare the ZF-violated scheme with the proposed method to demonstrate the impact of cross-correlation constraints on overall performance, it is also necessary to consider communication performance.

Fig. 5 unfolds the average achievable communication rate versus communication SNR under the same settings as in Fig. 4. It is observed that the communication-only scheme achieves the best average communication rate, while other schemes experience communication performance loss due to the sensing MI constraints. The propose method demonstrates superior average communication rate compared to the MI-constrained scheme. This is due to the fact that the MI-constrained approach optimizes the lower bound of SINR, which cannot attain the same communication performance as the proposed method that directly optimizes SINRs. Moreover, the performance gap between the proposed method and the communication-centric approach diminishes as SNR increases, converging closely at high SNR levels. We observe that the average communication rate of the proposed method closely approximates that of the ZF-violated scheme, suggesting that the cross-correlation constraints do not compromise the communication performance either.

In Fig. 6, we evaluate the tradeoff between the average communication rate and the sensing MI for $C = 2$ and $C = 3$. For the proposed method, the weight of sensing MI α varies from 0.1 to 0.9. The weights of different communication users are set with the same value, calculated by $\omega_i = (1 - \alpha)/C \quad \forall i \in \mathcal{C}$. The weights of different sensing targets are equivalently established as $\xi_k = \alpha/K \quad \forall k$. The threshold ρ utilized in the MI-constrained approach varies from 0.2 to 0.9. In the case where the number of users and targets are the same, the proposed method achieves higher sensing MI than the MI-constrained scheme with the same communication

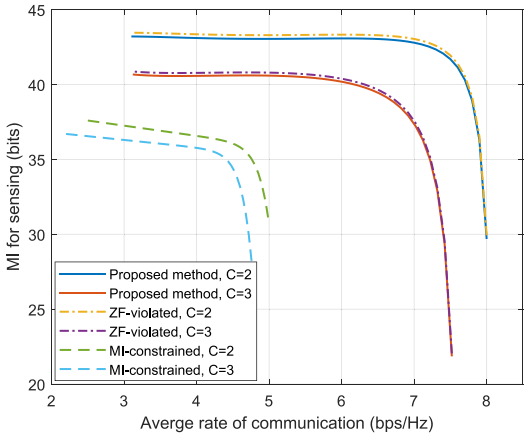

Fig. 6. Tradeoff between the sensing MI and the average rate of the MU-MIMO communication.

average rate. Similarly, when to achieve the same sensing MI, the proposed method obtains a better average communication rate. This indicates that the proposed method provides a better tradeoff between the multitarget sensing performance and multiuser communication performance compared to the MI-constrained scheme. It is also noted that the proposed method and the ZF-violated scheme exhibit a similar tradeoff, demonstrating that the cross-correlation constraints does not compromise the overall performance of the ISAC system. Furthermore, we observe that the more users the ISAC system has to communicate with reliably, the lower the sensing MI is achieved in the proposed method. This is because ensuring an additional communication user performance requires utilizing transmit power resources originally allocated for sensing.

Since, the sensing MI is not the only performance measure for sensing, we also examine the angle estimation performance obtained by using the Capon method. We simulate the two radar targets located at the directions 20° and 40°, respectively. The complex amplitude of the targets are both 1 [13]. Fig. 7 exhibits the Capon spatial spectrum with and without transmitting radar signals for several benchmarks in one test. Without transmitting the radar signals, it can be observed from Fig. 7(a), (c), (e), and (f) that the proposed method exhibits an angular resolution close to that of the radar-only approach and yields significantly higher peak values at the desired target directions compared to the other ZF-violated and MI-constrained schemes. We also observe that when the number of targets does not exceed the number of users, all the schemes can effectively detect and estimate the targets regardless of whether additional radar signals are transmitted.

Then, we consider the scenario where there are three targets, with two of them placed closely. The directions of the targets are 0°, 5°, and 40°, and the complex amplitude for each target is 1 [13]. When transmitting the radar signals, it can be observed that the peak at the location of 0° in Fig. 8(d) is not prominent compared with Fig. 8(b), resulting in an inadequate resolution of two closely spaced targets. This observation highlights that the proposed method enhances the ability to resolve multiple targets by suppressing the cross-correlation among the signals reflected from different targets

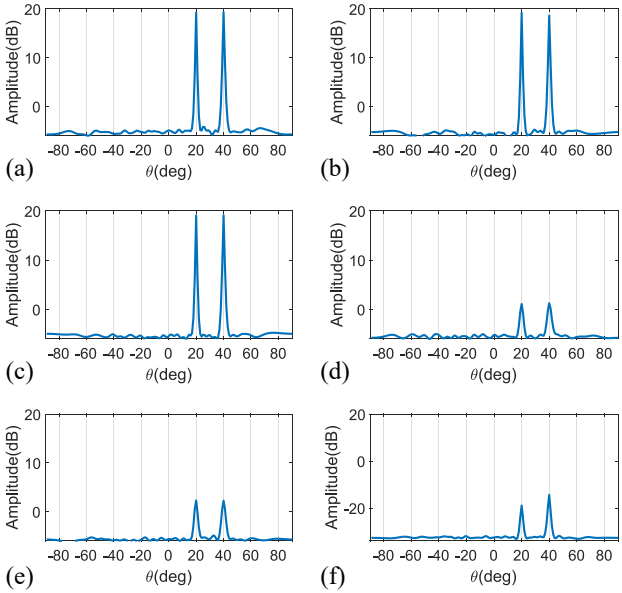

Fig. 7. Capon spatial spectrum for $K = 2$. (a) Capon spatial spectrum for the radar-only approach without radar signals. (b) Capon spatial spectrum for the proposed method. (c) Capon spatial spectrum for the proposed method without radar signals. (d) Capon spatial spectrum for the ZF-violated scheme. (e) Capon spatial spectrum for the ZF-violated scheme without radar signals. (f) Capon spatial spectrum for the MI-contrained scheme.

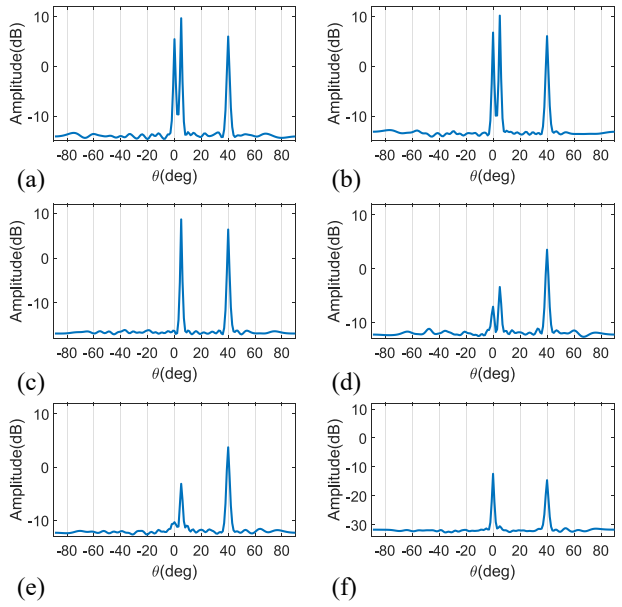

Fig. 8. Capon spatial spectrum for $K = 3$. (a) Capon spatial spectrum for the radar-only approach. (b) Capon spatial spectrum for the proposed method. (c) Capon spatial spectrum for the proposed method without radar signals. (d) Capon spatial spectrum for the ZF-violated scheme. (e) Capon spatial spectrum for the ZF-violated scheme without radar signals. (f) Capon spatial spectrum for the MI-contrained scheme.

through (27c). Additionally, it can be observed from Fig. 8(c), (e), and (f) that when the BS transmits only communication signals, all the three targets cannot be effectively distinguished, with only two of them exhibiting significant peaks. This is due to the fact that when only communication signals are transmitted, the rank of the transmitted signal covariance

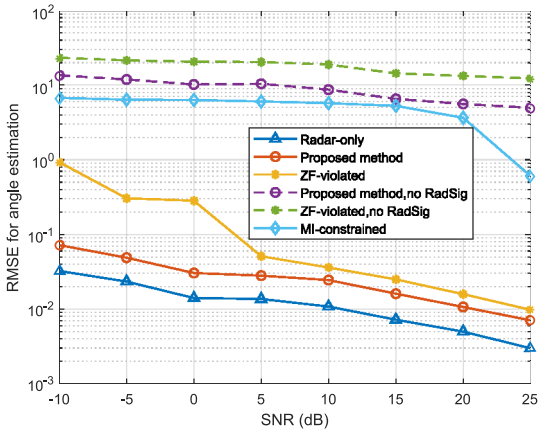

Fig. 9. RMSE for angle estimation versus receive SNR for $K = 3$.

matrix is limited by C, which cannot provide sufficient DoFs to form three beams to cover all the three targets.

Fig. 9 shows the root-mean-square-error (RMSE) of target angle estimation versus radar SNR. The angles of targets are estimated by finding the peaks in the Capon spatial spectrum. When the radar signals are not transmitted, the RMSE for the proposed scheme, the ZF-violated scheme, and the MI-constrained scheme is significantly higher compared to the other schemes that utilize the radar signals. This is due to the insufficient DoFs, often resulting in the inability to detect targets close to the true target direction, which aligns with the conclusion in Fig. 8. Additionally, we observe that when the radar signals are transmitted, the proposed scheme exhibits a lower RMSE compared to the ZF-violated scheme and is close to the radar-only scheme. This indicates that even with similar capabilities in maximizing sensing MI, the proposed scheme outperforms ZF-violated in terms of angular estimation performance. Therefore, the sensing MI upper bound with the cross-correlation constraints is more appropriate performance metric for the multitarget sensing.

VI. Conclusion

In this article, we investigated a multiobjective optimization framework for ISAC beamforming that provides a flexible tradeoff between multiple targets sensing and multiuser communication. We formulate a MOOP based on the tight upper bound of sensing MI and each user's SINR. Then, we employ a max-min utility function method to obtain specific Pareto optimal solutions while considering fairness between the users and sensing targets. Numerical results were presented for validating the proposed beamforming method and provided the useful insights. First, the proposed method can achieve superior performance boundaries of communication and sensing performance, while also facilitating a flexible tradeoff between them. Second, the proposed method can enhance target resolution and angle estimation accuracy for multiple targets, thereby validating the suitability of constrained sensing MI upper bound as a performance metric for multitarget sensing.

Extending the proposed framework to practical scenarios with imperfect channel state information (CSI) may degrade the communication and sensing performance, necessitating the development of the robust beamforming techniques that account for channel uncertainties. Additionally, dynamic target tracking in nonideal conditions can be computationally demanding, requiring the development of the low-complexity tracking algorithms and efficient beamforming update schemes. Future research should focus on investigating the robustness of the MI-based beamforming method under imperfect CSI and developing advanced techniques to mitigate its impact while enabling real-time adaptation for practical implementation.

Appendix A
Proof of Theorem 1

Substituting (10) into (12), the sensing MI can be simplified to (42), shown at the bottom of the page. The derivation of (42b) follows the fact that $\mathrm{vec}(\mathbf{ABC}) = (\mathbf{C}^{\mathrm{T}} \otimes \mathbf{A})\mathrm{vec}(\mathbf{B})$.

Then, by introducing the auxiliary block matrices

$$\mathbf{T} = \frac{1}{\sigma_r^2}\left[\mathrm{vec}\left(\mathbf{A}(\theta_1)\left(\mathbf{X}\mathbf{X}^H\right)\right), \ldots, \mathrm{vec}\left(\mathbf{A}(\theta_K)\left(\mathbf{X}\mathbf{X}^H\right)\right)\right]$$
$$\mathbf{M} = \left[\sigma_1^2\mathrm{vec}(\mathbf{A}(\theta_1)), \ldots, \sigma_K^2\mathrm{vec}(\mathbf{A}(\theta_K))\right]^H \tag{43}$$

the sensing MI in (42b) can be rewritten as

$$I\left(\tilde{\mathbf{y}}_r; \tilde{\mathbf{g}}\middle|\tilde{\mathbf{X}}\right) = \log[\det(\mathbf{I} + \mathbf{TM})] = \log[\det(\mathbf{I} + \mathbf{MT})] \tag{44}$$

where the final equality follows from the Sylvester's determinant identity $\det(\mathbf{I} + \mathbf{AB}) = \det(\mathbf{I} + \mathbf{BA})$. The (i, j)th entry of $\mathbf{MT}$ is given by

$$[\mathbf{MT}]_{i,j} = \frac{\sigma_i^2}{\sigma_r^2}\mathrm{vec}^H(\mathbf{A}(\theta_i))\mathrm{vec}\left(\mathbf{A}\left(\theta_j\right)\left(\mathbf{X}\mathbf{X}^H\right)\right)$$
$$= \frac{L\sigma_i^2}{\sigma_r^2}\mathrm{tr}\left(\mathbf{A}^H(\theta_i)\mathbf{A}\left(\theta_j\right)\mathbf{R}_X\right) = \sigma_i^2[\Phi]_{i,j} \tag{45}$$

where the derivation of (45) utilizes the identity $\mathrm{vec}^H(\mathbf{A})\mathrm{vec}(\mathbf{B}) = \mathrm{tr}(\mathbf{A}^H\mathbf{B})$, and $[\Phi]_{i,j}$ denotes the (i, j)th element of the matrix $\Phi \in \mathbb{C}^{K\times K}$. Next, we define a diagonal matrix $\Lambda \in \mathbb{C}^{K\times K}$ as

$$\Lambda \triangleq \mathrm{diag}\left\{\frac{1}{\sigma_1^2}, \frac{1}{\sigma_2^2}, \ldots, \frac{1}{\sigma_K^2}\right\}. \tag{46}$$

$$I\left(\tilde{\mathbf{y}}_r; \tilde{\mathbf{g}}\middle|\tilde{\mathbf{X}}\right) = \log\left[\det\left(\mathbf{I} + \frac{1}{\sigma_r^2}\left(\sum_{t=1}^{K}\sigma_k^2\left(\mathbf{X}^*\mathbf{X}^{\mathrm{T}} \otimes \mathbf{I}_{N_r}\right)\mathrm{vec}(\mathbf{A}(\theta_k))\mathrm{vec}(\mathbf{A}(\theta_k))^H\right)\right)\right] \tag{42a}$$
$$= \log\left[\det\left(\mathbf{I} + \frac{1}{\sigma_r^2}\left(\sum_{t=1}^{K}\sigma_k^2\mathrm{vec}\left(\mathbf{A}(\theta_k)\left(\mathbf{X}\mathbf{X}^H\right)\right)\mathrm{vec}(\mathbf{A}(\theta_k))^H\right)\right)\right] \tag{42b}$$

By extracting the constant coefficient terms $\{\sigma_1^2, \ldots, \sigma_K^2\}$ from determinant by row, the sensing MI is recast as

$$I\left(\tilde{\mathbf{y}}_r; \tilde{\mathbf{g}} \middle| \tilde{\mathbf{X}}\right) = \log\left[\det(\Phi + \Lambda) \prod_{k=1}^{K} \sigma_k^2\right] \tag{47}$$

which completes the proof of Lemma 1.

Appendix B
Proof of Lemma 2

We first prove that $\mathcal{M}$ is a compact set. Following [42], we know that the feasible transmit strategy set $\mathcal{R}$ is compact. According to [46], the continuous mapping of a compact set is also a compact set. Since, the upper bound of sensing MI I_{up} and each user's SINR γ_i are all the continuous functions of $\{\mathbf{R}_1, \ldots, \mathbf{R}_{C+M}\} \in \mathcal{R}$, and $\mathcal{M}$ is a compact set.

To prove that $\mathcal{M}$ is a normal set, we use a similar method as described in [14, Appx.A]. Take $\mathbf{x} = (I_{\text{up}}, \gamma_1, \ldots, \gamma_C) \in \mathcal{M}$ and assume that $(\mathbf{R}_1, \ldots, \mathbf{R}_{C+M})$ is a feasible strategy that attains the point $\mathbf{x}$. Our goal is to prove that any given $\mathbf{x}' = (I'_{\text{up}}, \gamma'_1, \ldots, \gamma'_C)$ satisfying $\mathbf{x}' \leq \mathbf{x}$ also belongs to $\mathcal{M}$.

To this end, we represent the transmit beamforming strategy in a new form $(p_1\mathbf{R}_1, \ldots, p_{C+M}\mathbf{R}_{C+M})$, where $(p_1, \ldots, p_{C+M}) \in \mathcal{P}$ is a set of power allocation coefficients that should belong to

$$\mathcal{P} = \{\ (p_1, \ldots, p_{C+M}) : p_n > 0, \operatorname{tr}\left(\sum_{n=1}^{C+M} p_n \mathbf{R}_n\right) \leq P_T, \operatorname{tr}\left(\mathbf{a}(\theta_i)\mathbf{a}^H(\theta_j)\left(\sum_{n=1}^{C+M} p_n \mathbf{R}_n\right)\right) = 0 \quad (i \neq j)\ \}. \tag{48}$$

First, we need to find that $(p_1, \ldots, p_{C+M}) \in \mathcal{P}$ satisfies the given SINRs and I_{up}, i.e.,

$$\gamma_i = \frac{p_i \mathbf{h}_i^H \mathbf{R}_i \mathbf{h}_i}{\sum_{j=1, j\neq i}^{C+M} p_j \mathbf{h}_i^H \mathbf{R}_j \mathbf{h}_i + \sigma_c^2} \quad \forall i \in \mathcal{C} \tag{49a}$$

$$I_{\text{up}} = \sum_{k=1}^{K} \log\left(1 + \frac{N_r \sigma_k^2 L}{\sigma_r^2} \mathbf{a}^H(\theta_k)\left(\sum_{n=1}^{C+M} p_n \mathbf{R}_n\right)\mathbf{a}(\theta_k)\right). \tag{49b}$$

For (49a), given arbitrary $(p_{C+1}, \ldots, p_{C+M})$ satisfying each element $p_i \in (0, 1]$, we can derive the following equation, i.e.,:

$$\Gamma(\mathbf{A}_1\mathbf{p}_1 + \mathbf{A}_2\mathbf{p}_2 + \mathbf{b}) = \mathbf{p}_1 \tag{50}$$

where $\Gamma = \operatorname{diag}(\gamma_i, \ldots, \gamma_C)$, $\mathbf{p}_1 = [p_1, \ldots, p_C]^{\mathrm{T}}$, and $\mathbf{p}_2 = [p_{C+1}, \ldots, p_{C+M}]^{\mathrm{T}}$

$$\mathbf{A}_1 = \begin{bmatrix} 0 & a_{1,2} & \cdots & a_{1,C} \\ a_{2,1} & 0 & \cdots & a_{2,C} \\ \vdots & \vdots & \ddots & \vdots \\ a_{C,1} & a_{C,2} & \cdots & 0 \end{bmatrix} \tag{51}$$

$$\mathbf{A}_2 = \begin{bmatrix} a_{1,C+1} & \cdots & a_{1,C+M} \\ a_{2,C+1} & \cdots & a_{2,C+M} \\ \vdots & \ddots & \vdots \\ a_{C,C+1} & \cdots & a_{C,C+M} \end{bmatrix} \tag{52}$$

with

$$a_{i,j} = \frac{\mathbf{h}_i^H \mathbf{R}_j \mathbf{h}_i}{\mathbf{h}_i^H \mathbf{R}_i \mathbf{h}_i} \tag{53}$$

and $\mathbf{b} = [b_1, \ldots, b_C]^{\mathrm{T}} \in \mathbb{R}^{C\times 1}$ with

$$b_i = \frac{\sigma_c^2}{\mathbf{h}_i^H \mathbf{R}_i \mathbf{h}_i}. \tag{54}$$

Based on (50), we can obtain that

$$\begin{aligned} \mathbf{p}_1 &= (\mathbf{I} - \Gamma\mathbf{A}_1)^{-1}(\Gamma\mathbf{A}_2\mathbf{p}_2 + \Gamma\mathbf{b}) \\ &\overset{(a)}{=} \left(\mathbf{I} + \sum_{n=1}^{\infty} (\Gamma\mathbf{A}_1)^n\right)(\Gamma\mathbf{A}_2\mathbf{p}_2 + \Gamma\mathbf{b}) \end{aligned} \tag{55}$$

where (a) is based on the Neumann series approximation [47] of $(\mathbf{I} - \Gamma\mathbf{A}_1)^{-1}$. Since, all the elements in $\mathbf{A}_1$, $\mathbf{A}_2$, $\mathbf{p}_2$, and $\mathbf{b}$ are nonnegative, it indicates that each element in $\mathbf{p}_1$ is obtained from a polynomial with the positive coefficients in $\gamma_i, \ldots, \gamma_C$. Therefore, a decrease in γ_i will necessarily lead to a decrease in at least one of the power allocation coefficients $(p_1, \ldots, p_C)$. For (49b), I_{up} can be further rewritten as

$$I_{\text{up}} = \log\left(\prod_{k=1}^{K}\left(1 + \sum_{n=1}^{C+M} p_n d_{nk}\right)\right) \tag{56}$$

where d_{nk} is a positive constant given as

$$d_{nk} = \frac{N_r \sigma_k^2 L}{\sigma_r^2} \mathbf{a}^H(\theta_k)\mathbf{R}_n\mathbf{a}(\theta_k) \quad \forall n, k. \tag{57}$$

From (56), it is evident that I_{up} can be expressed as the logarithm of a polynomial in $p_1, \ldots, p_{C+M}$ with the positive coefficients. As the logarithm function is monotonically increasing, a reduction in I_{up} will inevitably result in a decrease in at least one of the power allocation coefficients $(p_1, \ldots, p_{C+M})$.

In summary, based on the above analysis, we can conclude that for any $\gamma'_i \leq \gamma_i \quad \forall i$ or $I'_{\text{up}} \leq I_{\text{up}}$, we can always properly find $\mathbf{p}' \in \mathcal{P}$ satisfying that $\mathbf{p}' \leq \mathbf{p}$, and making $(p'_1\mathbf{R}_1, \ldots, p'_{C+M}\mathbf{R}_{C+M})$ a feasible solution that attains the point $\mathbf{x}'$. This implies that if $\mathbf{x}' \in \mathbb{R}_+^n$ and satisfies $\mathbf{x}' \leq \mathbf{x}$, then $\mathbf{x}'$ belongs to $\mathcal{M}$. In other words, the achievable performance region $\mathcal{M}$ is a normal set, which completes the proof.

Appendix C
Proof of Theorem 2

The optimal values of (36) is denoted as $(I^*_{\text{up}}, \gamma_1^*, \ldots, \gamma_C^*)$, and the corresponding optimal solution with arbitrary ranks as

$$\left\{\mathbf{R}_1^*, \ldots, \mathbf{R}_{C+M}^*\right\}. \tag{58}$$

We need to prove that the rank-one optimal solution $\{\bar{\mathbf{R}}_1, \ldots, \bar{\mathbf{R}}_{C+M}\}$ can be constructed from (58). First, we construct $\{\bar{R}_1, \ldots, \bar{R}_C\}$ as

$$\bar{\mathbf{R}}_i = \bar{\mathbf{w}}_i \bar{\mathbf{w}}_i^H \quad \forall i \in \mathcal{C} \tag{59}$$

where

$$\bar{\mathbf{w}}_i = \frac{\mathbf{R}_i^* \mathbf{h}_i}{\sqrt{\mathbf{h}_i^H \mathbf{R}_i^* \mathbf{h}_i}} \quad \forall i \in \mathcal{C}. \tag{60}$$

It can be readily verified that

$$\mathbf{h}_i^H \bar{\mathbf{R}}_i \mathbf{h}_i = \mathbf{h}_i^H \bar{\mathbf{w}}_i \bar{\mathbf{w}}_i^H \mathbf{h} = \mathbf{h}_i^H \mathbf{R}_i^* \mathbf{h}_i \quad \forall i \in \mathcal{C}. \tag{61}$$

By noting the above fact, we next construct $\{\bar{\mathbf{R}}_{C+1}, \ldots, \bar{\mathbf{R}}_{C+M}\}$. Let $\mathbf{R}_r \triangleq \sum_{n=1}^{C+M} \mathbf{R}_n^* - \sum_{n=1}^{C} \bar{\mathbf{R}}_n = \sum_{n=C+1}^{C+M} \bar{\mathbf{R}}_n$. Therefore, we need to prove that $\mathbf{R}_r$ is semidefinite. Since, $\sum_{n=C+1}^{C+M} \mathbf{R}_n^*$ is semidefinite due to (27d), we only need to prove that $\mathbf{R}_i^* - \bar{\mathbf{R}}_i \succeq 0$ for all $i \leq C$.

For any $\mathbf{x} \in \mathbb{C}^{N_t}$, it holds that

$$\mathbf{x}^H \left(\mathbf{R}_i^* - \bar{\mathbf{R}}_i\right) \mathbf{x} = \mathbf{x}^H \mathbf{R}_i^* \mathbf{x} - \frac{\left|\mathbf{x}^H \mathbf{R}_i^* \mathbf{h}_i\right|^2}{\left(\mathbf{h}_i^H \mathbf{R}_i^* \mathbf{h}_i\right)}. \tag{62}$$

According to the Cauchy–Schwarz inequality, we have

$$\left(\mathbf{h}_i^H \mathbf{R}_i^* \mathbf{h}_i\right)\left(\mathbf{x}^H \mathbf{R}_i^* \mathbf{x}\right) \geq \left|\mathbf{x}^H \mathbf{R}_i^* \mathbf{h}_i\right|^2 \tag{63}$$

which means that

$$\mathbf{x}^H \left(\mathbf{R}_i^* - \bar{\mathbf{R}}_i\right) \mathbf{x} \geq 0 \quad \forall \mathbf{x} \in \mathbb{C}^N. \tag{64}$$

i.e., $\mathbf{R}_r \succeq 0$.

By taking the Cholesky decomposition of $\mathbf{R}_r$, we have

$$\bar{\mathbf{W}}_r \bar{\mathbf{W}}_r^H = \sum_{n=1}^{C+M} \mathbf{R}_n^* - \sum_{n=1}^{C} \bar{\mathbf{R}}_n \tag{65}$$

where $\bar{\mathbf{W}}_r = [\bar{\mathbf{w}}_{C+1}, \ldots, \bar{\mathbf{w}}_{C+M}]$ is a lower triangular matrix. So, we obtain that $\bar{\mathbf{R}}_j = \bar{\mathbf{w}}_j \bar{\mathbf{w}}_j^H$ for $j = C+1, \ldots, C+M$. It follows that:

$$\sum_{n=1}^{C+M} \mathbf{R}_n^* = \sum_{n=1}^{C+M} \bar{\mathbf{R}}_n. \tag{66}$$

Now, we need to validate that $\{\bar{\mathbf{R}}_1, \ldots, \bar{\mathbf{R}}_{C+M}\}$ is a feasible solution to (36). And we have

$$\begin{aligned} \mathrm{tr}\left(\sum_{n=1}^{C+M} \bar{\mathbf{R}}_n\right) &= \mathrm{tr}\left(\sum_{n=1}^{C+M} \mathbf{R}_n^*\right) \leq P_T \\ &= \mathrm{tr}\left(\mathbf{a}(\theta_i)\mathbf{a}^H(\theta_j)\left(\sum_{n=1}^{C+M} \bar{\mathbf{R}}_n\right)\right) \\ \mathrm{tr}\left(\mathbf{a}(\theta_i)\mathbf{a}^H(\theta_j)\left(\sum_{n=1}^{C+M} \mathbf{R}_n^*\right)\right) &= 0 (i \neq j) \end{aligned} \tag{67}$$

which means that (36) hold for $\{\bar{\mathbf{R}}_1, \ldots, \bar{\mathbf{R}}_{C+M}\}$.

Based on (61), we have

$$\begin{aligned} I_{\mathrm{up}}^* &= \sum_{k=1}^{K} \log\left(1 + \frac{N_r \sigma_k^2 L}{\sigma_r^2} \mathbf{a}^H(\theta_k)\left(\sum_{n=1}^{C+M} \mathbf{R}_n^*\right)\mathbf{a}(\theta_k)\right) \\ &= \sum_{k=1}^{K} \log\left(1 + \frac{N_r \sigma_k^2 L}{\sigma_r^2} \mathbf{a}^H(\theta_k)\left(\sum_{n=1}^{C+M} \bar{\mathbf{R}}_n\right)\mathbf{a}(\theta_k)\right) \end{aligned} \tag{68}$$

$$\begin{aligned} \gamma_i^* &= \frac{\mathbf{h}_i^H \mathbf{R}_i^* \mathbf{h}_i}{\mathbf{h}_i^H \left(\sum_{n=1}^{C+M} \mathbf{R}_n^*\right)\mathbf{h}_i - \mathbf{h}_i^H \mathbf{R}_i^* \mathbf{h}_i + \sigma_c^2} \\ &= \frac{\mathbf{h}_i^H \bar{\mathbf{R}}_i \mathbf{h}_i}{\mathbf{h}_i^H \left(\sum_{n=1}^{C+M} \bar{\mathbf{R}}_n\right)\mathbf{h}_i - \mathbf{h}_i^H \bar{\mathbf{R}}_i \mathbf{h}_i + \sigma_c^2} \end{aligned} \tag{69}$$

which means that the optimal values do not change.

Above all, $\{\bar{\mathbf{R}}_1, \ldots, \bar{\mathbf{R}}_{C+M}\}$ is also the optimal solution to (36), which completes the proof.

REFERENCES

[1] F. Liu, C. Masouros, A. P. Petropulu, H. Griffiths, and L. Hanzo, "Joint radar and communication design: Applications, state-of-the-art, and the road ahead," *IEEE Trans. Commun.*, vol. 68, no. 6, pp. 3834–3862, Feb. 2020.

[2] F. Liu et al., "Integrated sensing and communications: Toward dual-functional wireless networks for 6G and beyond," *IEEE J. Sel. Areas Commun.*, vol. 40, no. 6, pp. 1728–1767, Mar. 2022.

[3] D. Ma, N. Shlezinger, T. Huang, Y. Liu, and Y. C. Eldar, "Joint radar-communication strategies for autonomous vehicles: Combining two key automotive technologies," *IEEE Signal Process. Mag.*, vol. 37, no. 4, pp. 85–97, Jun. 2020.

[4] Z. Feng, Z. Wei, X. Chen, H. Yang, Q. Zhang, and P. Zhang, "Joint communication, sensing, and computation enabled 6G intelligent machine system," *IEEE Netw.*, vol. 35, no. 6, pp. 34–42, Nov. 2021.

[5] X. Li et al., "UAV-enabled multi-pair massive MIMO-NOMA relay systems with low-resolution ADCs/DACs," *IEEE Trans. Veh. Technol.*, vol. 73, no. 2, pp. 2171–2186, Feb. 2024.

[6] Y. Cheng, J. Du, J. Liu, L. Jin, X. Li, and D. B. da Costa, "Nested tensor-based framework for ISAC assisted by reconfigurable intelligent surface," *IEEE Trans. Veh. Technol.*, vol. 73, no. 3, pp. 4412–4417, Mar. 2024.

[7] J. A. Zhang et al., "An overview of signal processing techniques for joint communication and radar sensing," *IEEE J. Sel. Topics Signal Process.*, vol. 15, no. 6, pp. 1295–1315, Sep. 2021.

[8] J. A. Zhang et al., "Enabling joint communication and radar sensing in mobile networks—A survey," *IEEE Commun. Survs. Tuts.*, vol. 24, no. 1, pp. 306–345, 1st Quart., 2022.

[9] X. Fang, W. Feng, Y. Chen, N. Ge, and Y. Zhang, "Joint communication and sensing toward 6G: Models and potential of using MIMO," *IEEE Internet Things J.*, vol. 10, no. 5, pp. 4093–4116, 2023.

[10] Z. Wang, X. Mu, and Y. Liu, "Near-field integrated sensing and communications," *IEEE Commun. Lett.*, vol. 27, no. 8, pp. 2048–2052, Aug. 2023.

[11] F. Liu, C. Masouros, A. Li, H. Sun, and L. Hanzo, "MU-MIMO communications with MIMO radar: From co-existence to joint transmission," *IEEE Trans. Wireless Commun.*, vol. 17, no. 4, pp. 2755–2770, 2018.

[12] X. Liu, T. Huang, and Y. Liu, "Transmit design for joint MIMO radar and multiuser communications with transmit covariance constraint," *IEEE J. Sel. Areas Commun.*, vol. 40, no. 6, pp. 1932–1950, Mar. 2022.

[13] X. Liu, T. Huang, N. Shlezinger, Y. Liu, J. Zhou, and Y. C. Eldar, "Joint transmit beamforming for multiuser MIMO communications and MIMO radar," *IEEE Trans. Signal Process.*, vol. 68, pp. 3929–3944, Jun. 2020.

[14] L. Chen, F. Liu, W. Wang, and C. Masouros, "Joint radar-communication transmission: A generalized pareto optimization framework," *IEEE Trans. Signal Process.*, vol. 69, pp. 2752–2765, May 2021.

[15] Z. Ni, J. A. Zhang, K. Yang, X. Huang, and T. A. Tsiftsis, "Multi-metric waveform optimization for multiple-input single-output joint communication and radar sensing," *IEEE Trans. Commun.*, vol. 70, no. 2, pp. 1276–1289, Feb. 2022.

[16] X. Yuan et al., "Spatio-temporal power optimization for MIMO joint communication and radio sensing systems with training overhead," *IEEE Trans. Veh. Technol.*, vol. 70, no. 1, pp. 514–528, Jan. 2021.

[17] C. Meng, Z. Wei, and Z. Feng, "Adaptive waveform optimization for MIMO integrated sensing and communication systems based on mutual information," in *Proc. 14th Int. Conf. Wireless Commun. Signal Process. (WCSP)*, 2022, pp. 472–477.

[18] F. Liu, Y.-F. Liu, A. Li, C. Masouros, and Y. C. Eldar, "Cramér-Rao bound optimization for joint radar-communication beamforming," *IEEE Trans. Signal Process.*, vol. 70, pp. 240–253, 2022.

[19] H. Hua, X. Song, Y. Fang, T. X. Han, and J. Xu, "MIMO integrated sensing and communication with extended target: CRB-rate tradeoff," in *Proc. IEEE Glob. Commun. Conf.*, 2022, pp. 4075–4080.

[20] Z. Ren et al., "Fundamental CRB-rate tradeoff in multi-antenna ISAC systems with information multicasting and multi-target sensing," *IEEE Trans. Wireless Commun.*, vol. 23, no. 4, pp. 3870–3885, Apr. 2024.

[21] J. Sun, S. Ma, G. Xu, and S. Li, "Trade-off between positioning and communication for Millimeter wave systems with Ziv-Zakai bound," *IEEE Trans. Commun.*, vol. 71, no. 6, pp. 3752–3762, Jun. 2023.

[22] M. Bell, "Information theory and radar waveform design," *IEEE Trans. Inf. Theory*, vol. 39, no. 5, pp. 1578–1597, Sep. 1993.

[23] B. Tang and J. Li, "Spectrally constrained MIMO radar waveform design based on mutual information," *IEEE Trans. Signal Process.*, vol. 67, no. 3, pp. 821–834, Feb. 2019.

[24] Y. Yang and R. S. Blum, "MIMO radar waveform design based on mutual information and minimum mean-square error estimation," *IEEE Trans. Aerosp. Electron. Syst.*, vol. 43, no. 1, pp. 330–343, Jan. 2007.
[25] Y. Chen, Y. Nijsure, C. Yuen, Y. H. Chew, Z. Ding, and S. Boussakta, "Adaptive distributed MIMO radar waveform optimization based on mutual information," *IEEE Trans. Aerosp. Electron. Syst.*, vol. 49, no. 2, pp. 1374–1385, Apr. 2013.
[26] Z. Wei et al., "Waveform design for MIMO-OFDM integrated sensing and communication system: An information theoretical approach," *IEEE Trans. Commun.*, vol. 72, no. 1, pp. 496–509, Jan. 2024.
[27] F. Dong, F. Liu, S. Lu, and Y. Xiong, "Rethinking estimation rate for wireless sensing: A rate-distortion perspective," *IEEE Trans. Veh. Technol.*, vol. 72, no. 12, pp. 16876–16881, Dec. 2023.
[28] J. Li, G. Zhou, T. Gong, and N. Liu, "A framework for mutual information-based MIMO integrated sensing and communication beamforming design," *IEEE Trans. Veh. Technol.*, vol. 73, no. 6, pp. 8352–8366, Jun. 2024.
[29] J. Li and P. Stoica, "MIMO radar with colocated antennas," *IEEE Signal. Process. Mag.*, vol. 24, no. 5, pp. 106–114, Sep. 2007.
[30] D. Sarwate and M. Pursley, "Crosscorrelation properties of pseudorandom and related sequences," *Proc. IEEE*, vol. 68, no. 5, pp. 593–619, May 1980.
[31] R. Fritzsche and G. P. Fettweis, "Robust sum rate maximization in the multi-cell MU-MIMO downlink," in *Proc. IEEE Wireless Commun. Netw. Conf. (WCNC)*, 2013, pp. 3180–3184.
[32] F. Liu, L. Zhou, C. Masouros, A. Li, W. Luo, and A. Petropulu, "Toward dual-functional radar-communication systems: Optimal waveform design," *IEEE Trans. Signal Process.*, vol. 66, no. 16, pp. 4264–4279, Aug. 2018.
[33] J. M. F. Moura and Y. Jin, "Time reversal imaging by adaptive interference canceling," *IEEE Trans. Signal Process.*, vol. 56, no. 1, pp. 233–247, Jan. 2008.
[34] Z. Cheng, Z. He, B. Liao, and M. Fang, "MIMO radar waveform design with PAPR and similarity constraints," *IEEE Trans. Signal Process.*, vol. 66, no. 4, pp. 968–981, Feb. 2018.
[35] N. H. Lehmann et al., "Evaluation of transmit diversity in MIMO-radar direction finding," *IEEE Trans. Signal Process.*, vol. 55, no. 5, pp. 2215–2225, May 2007.
[36] M. Hua, Q. Wu, C. He, S. Ma, and W. Chen, "Joint active and passive beamforming design for IRS-aided radar-communication," *IEEE Trans. Wireless Commun.*, vol. 22, no. 4, pp. 2278–2294, Apr. 2023.
[37] Y. Liu, G. Liao, J. Xu, Z. Yang, and Y. Zhang, "Adaptive OFDM integrated radar and communications waveform design based on information theory," *IEEE Commun. Lett.*, vol. 21, no. 10, pp. 2174–2177, Oct. 2017.
[38] B. Tang, J. Tang, and Y. Peng, "MIMO radar waveform design in Colored noise based on information theory," *IEEE Trans. Signal Process.*, vol. 58, no. 9, pp. 4684–4697, Sep. 2010.
[39] P. Stoica, J. Li, and Y. Xie, "On probing signal design for MIMO radar," *IEEE Trans. Signal Process.*, vol. 55, no. 8, pp. 4151–4161, Aug. 2007.
[40] C. D. Meyer, *Matrix Analysis and Applied Linear Algebra*, vol. 71. Philadelphia, PA, USA: SIAM, 2000.
[41] E. Björnson, M. Bengtsson, and B. Ottersten, "Pareto characterization of the multicell MIMO performance region with simple receivers," *IEEE Trans. Signal Process.*, vol. 60, no. 8, pp. 4464–4469, Aug. 2012.
[42] E. Björnson, G. Zheng, M. Bengtsson, and B. Ottersten, "Robust monotonic optimization framework for Multicell MISO systems," *IEEE Trans. Signal Process.*, vol. 60, no. 5, pp. 2508–2523, Aug. 2012.
[43] Y. Ye, *Interior Point Algorithms: Theory and Analysis*. Hoboken, NJ, USA: Wiley, 2011.
[44] R. Senanayake, P. J. Smith, T. Han, J. Evans, W. Moran, and R. Evans, "Frequency permutations for joint radar and communications," *IEEE Trans. Wireless Commun.*, vol. 21, no. 11, pp. 9025–9040, Nov. 2022.
[45] C.-K. Wen, S. Jin, and K.-K. Wong, "On the sum-rate of multiuser MIMO uplink channels with jointly-correlated Rician fading," *IEEE Trans. Commun.*, vol. 59, no. 10, pp. 2883–2895, Oct. 2011.
[46] W. Rudin et al., *Principles of Mathematical Analysis*, vol. 3. New York, NY, USA: McGraw-Hill, 1976.
[47] G. W. Stewart, *Matrix Algorithms: Volume 1: Basic Decompositions*. Philadelphia, PA, USA: SIAM, 1998.

Chunwei Meng was born in China, in 1999. She received the B.E. degree from Beijing University of Posts and Telecommunications, Beijing, China, in 2021, where she is currently pursuing the Ph.D. degree.

Zhiqing Wei (Member, IEEE) received the B.E. and Ph.D. degrees from Beijing University of Posts and Telecommunications (BUPT), Beijing, China, in 2010 and 2015, respectively.

He is an Associate Professor with BUPT. He has authored one book, three book chapters, and more than 50 papers. His research interests include the performance analysis and optimization of intelligent machine networks.

Dr. Wei was granted the Exemplary Reviewer of IEEE Wireless Communications Letters in 2017 and the Best Paper Award of International Conference on Wireless Communications and Signal Processing in 2018. He was the Registration Co-Chair of IEEE/Chinese Institute of Communications (CIC) International Conference on Computer and Communications (ICCC) 2018 and the Publication Co-Chair of IEEE/CIC ICCC 2019 and IEEE/CIC ICCC 2020.

Dingyou Ma received the B.Sc. degree in aerospace science and technology from Xidian University, Xi'an, China, in 2016, and the Ph.D. degree in electronics engineering from Tsinghua University, Beijing, China, in 2022.

Since July 2022, he has been with the Key Laboratory of Universal Wireless Communications, Ministry of Education, School of Information and Communication Engineering, Beijing University of Posts and Telecommunications, Beijing, as a Lecturer. His current research interests include communications signal processing, radar signal processing, and dual-function radar-communications system.

Wanli Ni (Member, IEEE) received the B.Eng. and Ph.D. degrees from the School of Information and Communication Engineering, Beijing University of Posts and Telecommunications (BUPT), Beijing, China, in 2018 and 2023, respectively.

He is currently a Postdoctoral Research Associate with the Department of Electronic Engineering, Tsinghua University, Beijing. His research interests include federated learning, reconfigurable intelligent surface, over-the-air computation, semantic communication, performance analysis, and optimization of machine learning in wireless networks.

Dr. Ni was a recipient of the Outstanding Doctoral Dissertation Awards from China Education Society of Electronics and BUPT in 2023, the Excellent Graduate of Beijing in 2023, the BUPT Top-10 Campus Pioneers on Academic in 2023, the National Scholarship in 2022 and 2021, and the Samsung Scholarship in 2019. He was a recipient of the Best Paper Award from the IEEE SAGC Conference in 2020. He was a recipient of the IEEE ComSoc Student Travel Grant from multiple international conferences, including IEEE GLOBECOM, INFOCOM, and ICC. He was selected as an Exemplary Reviewer of the IEEE TRANSACTIONS ON COMMUNICATIONS in 2022, the IEEE COMMUNICATIONS LETTERS in 2022, and the IEEE WIRELESS COMMUNICATIONS LETTERS in 2023 and 2021. He has served as a Guest Editor of the Electronic journal special issue on *Edge Learning and Big AI Models in Wireless Communications and Networks*.

Liyan Su received the B.S.E. degree in electronics engineering and the Ph.D. degree in signal and information processing from Beihang University, Beijing, China, in 2010 and 2016, respectively.

He was a Visiting Researcher in electronics and computer science with the University of Southampton, Southampton, U.K., from 2013 to 2014. After graduation, he is currently with Research Department, Beijing Research and Development Subdivision, Wireless Network, Huawei Technologies Company Ltd., Beijing. His research interests include energy efficient and spectral efficient ultradense networks/massive MIMO systems and latency reduction techniques.

Zhiyong Feng (Senior Member, IEEE) received the B.S., M.S., and Ph.D. degrees in information and communication engineering from Beijing University of Posts and Telecommunications, Beijing, China, in 1993, 1997, and 2009, respectively.

She is currently a Full Professor. She is also the Director of the Key Laboratory of Universal Wireless Communications, Ministry of Education. Her research interests include wireless network architecture design and radio resource management in 5th-generation mobile networks, spectrum sensing and dynamic spectrum management in cognitive wireless networks, universal signal detection and identification, and network information theory.

Prof. Feng is a Technical Advisor of NGMN, an Editor of *IET Communications* and *KSII Transactions on Internet and Information Systems*, and a reviewer of IEEE TRANSACTIONS ON WIRELESS COMMUNICATIONS, IEEE TRANSACTIONS ON VEHICULAR TECHNOLOGY, and IEEE JOURNAL ON SELECTED AREAS IN COMMUNICATIONS. She is active in ITU-R, IEEE, ETSI, and CCSA standards.